

Response to Anonymous Referee #1

Thanks the reviewer for further reviewing our manuscript. All the comments raised by the reviewer have been answered carefully point-by point as below and the corresponding parts in the manuscript have been improved.

The original comments are copied here in black color.

Author's responses are in blue color.

All changes to the manuscript have been highlighted with red color in the submitted revised manuscript.

The revised paper addressed the major points in my previous comments. I recommend accept for the publication in ACP after further minor revisions as outlined below.

1. Line 145, “with small change magnitude” rewritten as “less changed”

Response: Corrected (Line 141).

2. Line 146-147, “the meteorological conditions ... considered” changed to “the meteorological conditions contributing to the atmospheric ventilation should be taken into consideration”

Response: Above mentioned suggestion has been corrected in manuscript at line 143-144

3. Line 151, delete “However”

Response: Corrected (Line 148)

4. Line 152-154, “To quantitatively ... coefficient” repeat above sentence, please delete it.

Response: Thank you very much for your valuable comments. This sentence has been deleted (Line 148-151).

5. Line 188, “the anomalies...”, better written as “composite anomalies...”. To my understanding, composite anomalies were the departure of the mean wind vectors and GH at 700 hPa averaged over the eight deteriorating air quality events from their respective means from Jan 1 2006 to Dec 31 2012 and from Jan 1 2014 to Feb 28 2017

Response: Agreed and corrected in manuscript at line 185-186.

6. Line 188, delete “over there”

Response: Corrected (Line 185)

7. Line 253, delete “Soon”, rewrite sentence as “As shown in Fig. 4b, a low trough was subsequently generated...”

Response: Corrected (Line 251)

8. Line 300, “composite anomalies”

Response: Agreed and corrected in manuscript at line 298 and all similar expressions in the supplement have also been revised.

9. Line 305, temperature change or temperature? Below you said “temperature”

Response: Represents “temperature change”. In order to avoid the ambiguity, the related instruction has been added in manuscript at line 304.

10. Line 313-314, “that the” changed to “characterized by the weak effects...”, delete “were weak”

Response: Agreed and corrected in manuscript at line 312-313.

11. Line 316, “with small change magnitude” change to “less altered”

Response: Agreed and corrected in manuscript at line 315-316.

12. Line 318, delete “magnitudes of”

Response: Corrected (Line 318).

13. Line 318-319, “the change of magnitudes of temperature” changed to “the degree of change in temperature”

Response: Corrected (Line 318-319).

14. Line 341, delete “in”

Response: Corrected (Line 341).

15. Line 345-368, this part is beyond scope of this paper because you were discussing “low pressure system”. You might briefly mention the firework and CNY influence but not such the details.

Response: This part has been properly refined in manuscript at line 347-374 according to your comments.

1 **Impact of low-pressure systems on winter heavy air pollution in the northwest Sichuan Basin, China**

2 Guicai Ning^{1,4}, Shigong Wang^{2,1}, Steve Hung Lam Yim^{3,4,5}, Jixiang Li¹, Yuling Hu¹, Ziwei Shang¹, Jinyan Wang¹,
3 Jiaxin Wang²

4 ¹The Gansu Key Laboratory of Arid Climate Change and Reducing Disaster, College of Atmospheric Sciences,
5 Lanzhou University, Lanzhou 730000, China

6 ²Key Laboratory of Education Bureau of Sichuan Province for Mountain Environmental Meteorology and Public
7 Health, School of Atmospheric Sciences, Chengdu University of Information Technology, Chengdu 610225, China

8 ³Department of Geography and Resource Management, The Chinese University of Hong Kong, Hong Kong, China

9 ⁴The Institute of Environment, Energy and Sustainability, The Chinese University of Hong Kong, Hong Kong, China

10 ⁵Stanley Ho Big Data Decision Analytics Research Centre, The Chinese University of Hong Kong, Shatin, N.T.,
11 Hong Kong, China

12 Correspondence to: Shigong Wang (wangsg@cuit.edu.cn, wangsg@lzu.edu.cn)

13 **Abstract**

14 The cities of Chengdu, Deyang, and Mianyang in the northwest Sichuan Basin are part of a rapidly developing
15 urban agglomeration adjoining the eastern slopes of the Tibetan Plateau. Heavy air pollution events have frequently
16 occurred over the cities in recent decade, but the effects of meteorological conditions on these pollution events are
17 unclear. We explored the effects of weather systems on winter heavy air pollution from 1 January 2006 to 31
18 December 2012 and from 1 January 2014 to 28 February 2017. Ten heavy air pollution events occurred during the
19 research period and eight of these took place while the region was affected by a dry low-pressure system at 700 hPa.
20 When the urban agglomeration was in front of the low-pressure system and the weather conditions were controlled
21 by a warm southerly air flow, and a strong temperature inversion appeared above the atmospheric boundary layer
22 acting as a lid. Forced by this strong inversion layer, the local secondary circulation was confined within the
23 atmospheric boundary layer and the horizontal wind speed in the lower troposphere was low. As a result, vertical
24 mixing and horizontal dispersion in the atmosphere were poor, favoring the formation of heavy air pollution events.
25 After the low-pressure system had transited over the region, the weather conditions in the urban agglomeration were
26 controlled by a dry and cold air flow from the northwest at 700 hPa. The strong inversion layer gradually dissipated,

27 the secondary circulation enhanced and uplifted, and the horizontal wind speed in the lower troposphere also
28 increased, resulting in a sharp decrease in the concentration of air pollutants. The strong inversion layer above the
29 atmospheric boundary layer induced by the low-pressure system at 700 hPa thus played a key role in the formation
30 of heavy air pollution during the winter months in this urban agglomeration. This study provides scientific insights
31 for forecasting heavy air pollution in this region of China.

32 **1 Introduction**

33 Air quality, especially the occurrence of heavy air pollution events, is not only strongly affected by excessive
34 emission of air pollutants, but is also closely associated with meteorological conditions, including atmospheric
35 circulations, weather systems, structures of atmospheric boundary layer, and the corresponding meteorological
36 parameters (**Deng et al., 2014;Gu and Yim, 2016;Li et al., 2015;Wei et al., 2011;Ye et al., 2016;Zhang et al.,**
37 **2012a**). The total amount of pollutants emitted in a particular period of time is usually stable in China (**Wu et al.,**
38 **2017**), but there are large differences in the concentrations of air pollutants, indicating that the meteorological
39 conditions have an important role in modulating concentrations of ambient air pollutants (**Gao et al., 2011;Hu et al.,**
40 **2014;Ji et al., 2014;Ji et al., 2012;Wang et al., 2010;Wang et al., 2009;Yang et al., 2011**).

41 Weather systems control the ability of the atmosphere to disperse pollutants and thus provide the primary
42 driving force for variations in regional air pollution (**Chen et al., 2008;Ye et al., 2016**). Leśniok et al. (2010)
43 reported that the atmosphere was stagnant and that the concentrations of near-ground air pollutants increased
44 significantly in Upper Silesia, Poland during periods with an anticyclonic circulation. By contrast, when a cyclonic
45 circulation prevailed, causing an inflow of fresh air masses from regions with lower levels of pollution, the
46 concentrations of air pollutants decreased. As synoptic-scale high-pressure ridges at 500 hPa transit across Utah,
47 accompanied by warm advection above valleys, the stability of the atmosphere is increased and favors the formation
48 of persistent pools of cold air, resulting in deterioration in air quality (**Whiteman et al., 2014**).

49 Many studies have been carried out on the impact of weather systems on air quality in China. Bei et al. (2016)

50 classified typical synoptic situations and evaluated their contributions to air quality in the Guanzhong Basin, China.
51 They found that an inland high-pressure system at 850 hPa resulted in temperature inversion, low horizontal wind
52 speed and a shallow atmospheric boundary layer, which favor the formation of heavy air pollution. Weather systems
53 have significantly impact on the transport of air pollutants. Luo et al. (2018) reported that the trans-boundary air
54 pollution and the pollutant concentration in Hong Kong increased when a tropical cyclones is approaching. During
55 winter, floating dust particles over northwestern China can be carried downstream to northern China by the
56 prevailing northwesterly winds at 700 hPa, where they mix with anthropogenic pollution to form a regional haze
57 (**Tao et al., 2012;Tao et al., 2014**). Changes in weather systems also significantly influence air quality. Shallowing
58 of the East Asian trough and weakening of the Siberian high-pressure in winter can induce weak horizontal
59 advection and vertical convection in the lower troposphere, reducing the height of the boundary layer in the
60 Beijing–Tianjin–Hebei region and favoring the formation of haze (**Zhang et al., 2016**).

61 The deep Sichuan Basin to the east of the Tibetan Plateau has a maximum elevation difference >2000 m, and is
62 ranked fourth in China for heavy air pollution after the Beijing–Tianjin–Hebei region, the Yangtze River Delta, and
63 the Pearl River Delta (**Tian et al., 2017;Zhang et al., 2012b**). The complex terrain leads to unique weather systems
64 that affect air quality in this region (**Chen et al., 2014;Huang et al., 2017**). Low-pressure systems, such as a
65 southwest vortex and low trough, are often formed at 700 hPa due to the dynamic and thermodynamic effects of the
66 Tibetan Plateau (**Wang and Tan, 2014;Yu et al., 2016**) and have different characteristics in different seasons. They
67 are warm and moist low-pressure systems in summer and autumn and have crucial effects on local precipitation
68 (**Feng et al., 2016;Peng and Cheng, 1992**); much work has been carried out in an attempt to understand the impacts
69 of these low-pressure systems on precipitation (**Chen et al., 2015;Fu et al., 2011;Kuo et al., 1986;Kuo et al.,**
70 **1988;Ni et al., 2017**). In winter and spring, however, these low-pressure systems are both dry and cold (**Feng et al.,**
71 **2016**). No attempt has previously been made to investigate the association between air quality and these dry and cold
72 low-pressure systems.

73 Chengdu, Deyang, and Mianyang, have undergone rapid development to form an urban agglomeration in the
74 northwest Sichuan Basin. This urban agglomeration lies close to the eastern slopes of Tibetan Plateau, and is affected
75 by low-pressure systems moving east from the plateau (Feng et al., 2016). Heavy air pollution events have
76 frequently occurred over there in recent decade. Number of days with exceedance of Grade II standards (MEP, 2012)
77 is more than 150 days each year in Chengdu (Ning et al., 2018). Most previous studies have investigated the basic
78 characteristics of air pollution (Chen and Xie, 2012; Chen et al., 2014; Luo et al., 2001; Ning et al., 2018; Tao et al.,
79 2013a; Tao et al., 2013b; Zhang et al., 2017) and the related meteorological parameters (He et al., 2017; Li et al.,
80 2015; Liao et al., 2017; Zeng and Zhang, 2017). However, the influencing mechanism of dry low-pressure system
81 on heavy air pollution events has yet to be comprehensively explored. The main purpose of this study was to
82 statistically analyze the relationships between low-pressure systems and winter heavy air pollution events in this
83 urban agglomeration, and to explore the physical mechanisms involved in the formation of winter heavy air pollution.
84 This study can deepen our understanding of the meteorological causes of heavy air pollution events in winter, and
85 provide scientific insights that can be used by local governments to take effective measures to mitigate air pollution.

86 This paper is organized as follows. The data and methods are described in Section 2. Section 3 provides a
87 statistical analysis of the relationships between the low-pressure systems and winter heavy air pollution. Section 4
88 illustrates the physical mechanisms of the effect of weather systems on air pollution and our conclusions are
89 summarized in Section 5.

90 **2 Data and methods**

91 **2.1 Air quality data**

92 Air pollution in the Sichuan Basin during the winter months is mainly caused by particulate matter (Ning et al.,
93 2018). The Chinese Ministry of Environmental Protection (MEP) currently monitors particles with diameters ≤ 2.5
94 μm ($\text{PM}_{2.5}$) and particles with diameters $\leq 10 \mu\text{m}$ (PM_{10}). We studied heavy air pollution events occurring during the
95 winter months in Chengdu, Deyang, and Mianyang in the northwest Sichuan Basin (Fig. 1). We selected pollution

96 events with a daily PM_{10} mean concentration $\geq 350 \mu g m^{-3}$ from 1 January 2006 to 31 December 2012 and from 1
97 January 2014 to 28 February 2017. The third revision of the “Ambient Air Quality Standard” (AAQS)
98 (GB3095-2012) was released on February 29th, 2012, replacing the old “Ambient Air Quality Standard” (AAQS)
99 (GB3095-1996) and $PM_{2.5}$ was adopted into the AAQS in China since 2013. The air quality monitoring stations
100 needed to be updated and the data of air pollutants monitored in the three cities existed missing measurement during
101 2013. Thus, the winter heavy pollution events during 2013 have not been analyzed in this paper. Moreover, the PM_{10}
102 daily mean concentration from 1 January 2014 to 28 February 2017 refers to the 24-hour average concentration of
103 PM_{10} from 00:00 BST (Beijing Standard Time, i.e., Coordinate Universal Time (UTC) +8 h) to 24:00 BST on the
104 current day based on the new “Ambient Air Quality Standard” (AAQS) (GB3095-2012). However, based on the old
105 “Ambient Air Quality Standard” (AAQS) (GB3095-1996), the PM_{10} daily mean concentration from 1 January 2006
106 to 31 December 2012 refers to the 24-hour average concentration of PM_{10} from 12:00 BST on the previous day to
107 12:00 BST on the current day. Hourly concentrations of $PM_{2.5}$, sulfur dioxide (SO_2), nitrogen dioxide (NO_2), carbon
108 monoxide (CO), and ozone (O_3) were also measured in the three cities from 1 January 2014 to 28 February 2017.
109 These above air quality data were collected from the MEP website (<http://datacenter.mep.gov.cn/index>).

110 **2.2 Meteorological data**

111 **(1) ERA-Interim daily data**

112 To analyze the weather systems at 700 hPa, and the dynamic and thermodynamic conditions in the lower
113 troposphere, the temperature, the geopotential, the vertical velocity, and the u and v components of wind during the
114 study period were obtained from the ERA-Interim daily dataset ($0.125^\circ \times 0.125^\circ$ grids) from 950 to 500 hPa for a
115 total of 14 vertical layers (with a vertical separation of 25 hPa from 950 to 775 hPa and a vertical separation of 50
116 hPa from 750 to 500 hPa). These meteorological data are available for 00:00, 06:00, 12:00, and 18:00 UTC and were
117 collected from the website (<http://apps.ecmwf.int/datasets/data/interim-full-daily/levtype=pl/>). The height of the
118 atmospheric boundary layer was obtained from the ERA-Interim daily dataset at the surface with a 3 h temporal

119 resolution (00:00, 03:00, 06:00, 09:00, 12:00, 15:00, 18:00, and 21:00 UTC)
120 (<http://apps.ecmwf.int/datasets/data/interim-full-daily/levtype=sfc/>) to explore the structure of the atmospheric
121 boundary layer. This boundary layer height was defined as the level where the bulk Richardson number, based on the
122 difference between quantities at that level and the lowest model level, reaches the critical value $Ri_{cr} = 0.25$ (Beljaars,
123 2006).

124 (2) Sounding data

125 Radiosonde measurements from launches at Wenjiang station (see Fig. 1) in Chengdu city (30.70 °N, 103.83 °E,
126 elevation 541.0 m) at 08:00 and 20:00 BST were obtained from the University of Wyoming website
127 (<http://weather.uwyo.edu/upperair/sounding.html>) and included the temperature, potential temperature, and
128 horizontal wind. These data were used to investigate the dynamic and thermodynamic structure of the lower
129 troposphere.

130 2.3 Quantitative measures of meteorological conditions

131 2.3.1 Lower tropospheric stability

132 The lower tropospheric stability (LTS) is defined as the difference in the potential temperature between 700 hPa
133 and the surface (Slingo, 1987), and can be used to describe the thermodynamic state of the lower troposphere (Guo
134 et al., 2016a; Guo et al., 2016b). The LTS can be used to quantitatively evaluate the vertical mixing of air pollutants
135 in the lower troposphere:

$$136 \quad LTS = \theta_{700\text{hPa}} - \theta_{\text{surface}} \quad (1)$$

137 A large LTS represents a high degree of stability in the lower troposphere and indicates the potential for the weak
138 vertical mixing of air pollutants.

139 2.3.2 The mean wind speed in the lower troposphere

140 Sichuan Basin belongs to a low wind speed zone in China due to its deep mountain-basin topography, and the
141 wind speed in the mixing layer is often low and with ~~small change magnitudes~~ less changed (Chen and Xie,

142 **2012;Huang et al., 2017;Wang et al., 2018**). For analyzing air quality in Sichuan Basin, the meteorological
 143 conditions ~~in the lower troposphere that can reflect ventilation should be considered~~ contributing to the atmospheric
 144 ventilation should be taken into consideration. To quantitatively evaluate the horizontal dispersion of air pollutants in
 145 Sichuan Basin, the mean wind speed (MWS) in the lower troposphere was constructed based on the concept of
 146 ventilation coefficient (VC is a product of mixing layer height multiplied by average wind speed through the mixing
 147 height). In the eastern plains of China, the ventilation coefficient has been widely used to measure the capability of
 148 air pollutants' dispersion (**Deng et al., 2014;Lu et al., 2012;Tang et al., 2015**). ~~However, Thus, the meteorological~~
 149 ~~conditions above the mixing layer should also be considered in Sichuan Basin. To quantitatively evaluate the~~
 150 ~~horizontal dispersion of air pollutants in Sichuan Basin, the mean wind speed (MWS) in the lower troposphere was~~
 151 ~~constructed based on the concept of ventilation coefficient.~~The mean wind speed (MWS) in the lower troposphere
 152 was defined as:

$$153 \quad \text{MWS} = \frac{1}{h} \int_0^h V(z) dz \quad (2)$$

154 where h is the height above the ground at 700 hPa and $V(z)$ is the wind speed in the lower troposphere. This can
 155 be simplified as follows:

$$156 \quad \text{MWS} = \frac{1}{h} \sum_{i=1}^n [V_i(z_i) + V_{i-1}(z_{i-1})] \cdot 0.5 \cdot \Delta z_i \quad (3)$$

157 where n is the number of vertical layers from the ground surface to 700 hPa isobaric layer (including the 700 hPa
 158 isobaric layer, and n is greater than 6 in general), $V_i(z_i)$ is the wind speed in a vertical layer (when i=0 represents
 159 the wind speed at the ground surface and i=n represents the wind speed at 700 hPa), and Δz_i is the difference in
 160 height between the two adjacent vertical layers. A large value of MWS suggests strong horizontal dispersion of air
 161 pollutants.

162 **3 Heavy air pollution events and weather conditions**

163 **3.1 Overview of the heavy air pollution events**

164 A total of ten heavy winter air pollution events occurred from 1 January 2006 to 31 December 2012 and from 1
165 January 2014 to 28 February 2017 in the urban agglomeration of Chengdu, Deyang, and Mianyang. Nine events
166 were accompanied by a low-pressure system at 700 hPa, and the low-pressure systems in eight events were dry and
167 didn't induce precipitation. This paper explores the impacts of dry low-pressure systems on the eight winter heavy
168 air pollution events (see **Table 1** for a summary of these eight events).

169 **Table 1** shows that particulate matter was the primary pollutants during these eight heavy air pollution events.
170 Six of the eight events were classified as persistent air pollution events. A “persistent” pollution event was defined
171 by two or more consecutive days with daily PM₁₀ mean concentration $\geq 250 \mu\text{g m}^{-3}$, which is reported to be harmful
172 to the health of local residents (**Chow et al., 2006;Guo et al., 2016c;Langrish et al., 2012;Lim et al., 2012**), and
173 the longest duration was 10 days. Most of the heavy air pollution events had the characteristics of regional pollution,
174 with five pollution events occurring in multiple cities. Two heavy air pollution events (events 6 and 7) occurred
175 during the Spring Festival, with maximum daily mean PM₁₀ concentrations up to 403 and 562 $\mu\text{g m}^{-3}$ on the Chinese
176 New Year Day. This suggests that the centralized letting-off of fireworks during the traditional Chinese Spring
177 Festival, accompanied by poor conditions for the dispersion of air pollution, may lead to a sharp increase in the
178 concentration of particulate pollutants near ground level within a short period of time (**Huang et al., 2012;Liao et al.,**
179 **2017;Shi et al., 2011;Wang et al., 2007**).

180 **3.2 Weather systems and meteorological conditions during heavy air pollution events**

181 An analysis of the synoptic conditions showed that the urban agglomeration was affected by low-pressure
182 systems (low vortex or low trough) at 700 hPa during periods of deteriorating air quality in the eight heavy air
183 pollution events (**Fig. 2**). These studied areas were all located in front of low-pressure systems (east of low-pressure
184 systems) and were controlled by a southerly warm air flow (**Fig. 2**). To explore the differences between these

185 low-pressure systems and the background of winter atmospheric circulation—over there, composite anomalies~~the~~
186 anomalies of wind vectors and geopotential heights at 700 hPa were calculated (**Fig. S1**). The calculation method is
187 as follows: the averaged wind vectors and geopotential heights at 700 hPa during periods of deteriorating air quality
188 in the above eight events subtracted from their winter mean values from 1 January 2006 to 31 December 2012 and
189 from 1 January 2014 to 28 February 2017. As illustrated in **Fig. S1**, the anomalies of geopotential heights were
190 negative in the northwest of the urban agglomeration during periods of deteriorating air quality in these heavy air
191 pollution events. As a result, this urban agglomeration was located in front of an anomalous cyclone and was
192 controlled by a strong southerly anomaly wind (**Fig. S1**).

193 Weather systems can be characterized by their relative vorticity. A positive relative vorticity usually
194 corresponds to a low-pressure system, whereas a negative relative vorticity usually represents a high-pressure system.
195 Thus the relative vorticity at 700 hPa was analyzed during periods of both deteriorating and improving air quality
196 (**Table 2**). As shown in **Table 2**, the relative vorticities at 700 hPa during periods of deteriorating air quality were all
197 positive. This indicated that the study areas were located in front of low-pressure systems at 700 hPa. As a result, a
198 southerly warm air flow dominated at 700 hPa and led to an increase in temperature above the atmospheric boundary
199 layer, which increased atmospheric stability and favored the formation of an air pollution event. During periods of
200 improving air quality, the relative vorticities at 700 hPa of six heavy air pollution events (except for events 6 and 7)
201 were negative, showing that the low-pressure systems had transited across the study areas. These areas were thus
202 controlled by a northerly dry, cold air flow at 700 hPa. As a consequence, the temperature above the atmospheric
203 boundary layer decreased and the stability of the atmosphere weakened, which favored the vertical mixing of air
204 pollutants.

205 To explore the impacts of low-pressure systems on the structure of the atmospheric boundary layer, the
206 boundary layer height during periods of deteriorating and improving air quality were analyzed for each heavy air
207 pollution event (**Table 3**). In most of the heavy air pollution events, the height of the boundary layer increased after

208 the low-pressure system had passed across the study area. However, the increase in the height of the boundary layer
209 was not as significant as that seen in Eastern China (He et al., 2015; Ji et al., 2012; Leng et al., 2016; Qu et al.,
210 2017; Quan et al., 2013) and the boundary layer heights in air pollution events 3, and 4 decreased after transit of the
211 low-pressure system. These results show that the effects of the transit of low-pressure systems at 700 hPa on the
212 height of the boundary layer were weak, and the causes for the formation of these features will be discussed later. It
213 is therefore difficult to explain the variations in the concentrations of air pollutants in the study areas by considering
214 only the meteorological conditions within the boundary layer.

215 Previous studies have shown that the meteorological conditions above the boundary layer should also be
216 considered (Guo et al., 2016a; Guo et al., 2016b; Slingo, 1987). Therefore an index of the MWS in the lower
217 troposphere was proposed and this index, together with the LTS of the eight heavy air pollution events, were further
218 investigated (Table 3). The differences in the potential temperature between 700 hPa and the surface during periods
219 of deteriorating air quality in the eight events were all ≥ 18.54 K and the maximum value was 29.45 K, indicating that
220 the lower troposphere was very stable. The MWS was ≤ 4.22 m s⁻¹ for all eight events, with a minimum of 1.91 m s⁻¹.
221 These results show that the low-pressure systems resulted in the stagnation of air in the lower troposphere. After the
222 low-pressure systems had transited the study area, the lower tropospheric stability significantly decreased, with a
223 maximum decrease in the LTS of up to -11.23 K, and the MWS increased. This showed that the arrival of a dry, cold
224 air flow induced by the transit of the low-pressure system significantly weakened the stability of the lower
225 troposphere and increased the wind speed, improving air quality.

226 In events 6 and 7, however, although the study areas were still located in front of the low-pressure system and
227 the capacity for dispersion had not yet improved, the concentrations of particulate matter began to sharply decrease
228 before the transit of the low-pressure system. Both of these events occurred during the Chinese Spring Festival. After
229 the Chinese New Year Day, the letting-off of fireworks stopped and the emission of air pollutants was significantly
230 reduced, resulting in a sharp decrease in the concentration of particulate matter (Liao et al., 2017; Shi et al.,

231 **2011;Wang et al., 2007**). The decrease in the magnitude of the daily mean concentration of PM₁₀ in event 7 was up
232 to 350 μg m⁻³. These eight heavy air pollution events in the northwest Sichuan Basin can therefore be categorized
233 into two types based on their date of occurrence. The two heavy air pollution events (6 and 7) occurring during the
234 Chinese Spring Festival were categorized as Spring Festival excessive emission heavy air pollution events. The other
235 six events (events 1–5 and 8) were categorized as normal heavy air pollution events.

236 **4 Impacts of low-pressure systems on heavy air pollution events**

237 To further explore the mechanism involved in the formation of heavy air pollution events, with a particular
238 emphasis on the effect of low-pressure systems on air quality, a typical event was selected from the eight events
239 described in the preceding section. The variations in air quality and the dynamic and thermodynamic conditions in
240 the lower troposphere of the selected event were analyzed. Additionally, the impacts of Spring Festival excessive
241 emission on heavy air pollution events were also investigated.

242 **4.1 The influencing mechanism of low-pressure systems on heavy air pollution events**

243 Heavy air pollution event 8 occurred from 1 January 2017 to 6 January 2017 (Table 3) and the most polluted
244 area was Chengdu. The maximum daily mean concentrations of PM_{2.5} and PM₁₀ occurred on 5 January 2017. The
245 maximum PM₁₀ daily mean concentration in Chengdu was up to 480 μg m⁻³. The concentrations of particulate
246 matter increased sharply (**Fig. 3**) from 00:00 BST on 3 January 2017 to 00:00 BST on 5 January 2017 and the
247 concentrations of nitrogen dioxide and carbon monoxide also showed an increasing trend. Since 12:00 BST on 5
248 January 2017, the concentrations of particulate matter decreased significantly (**Fig. 3**).

249 **Fig. 4** shows the weather maps at 700 hPa during event 8. **Fig. 4a** shows that there was no low-pressure system
250 at 700 hPa over the urban agglomeration at 02:00 BST on 2 January and there was a dry, cold air flow from the
251 northwest. ~~Soon, a~~ **As** shown in **Fig. 4b**, a low trough was subsequently generated at 700 hPa on the west side of the
252 urban agglomeration at 14:00 BST on 2 January 2017, which showed the beginning of low-pressure system causing
253 air pollution. This trough later developed and was enhanced, and the lifespan of this low-pressure system was about

254 3 days. The urban agglomeration was still located at the front of the trough and was controlled by a warm, moist air
255 flow from the southwest until 02:00 BST on 5 January 2017 (**Fig. 4b** and **4c**). The concentrations of particulate
256 matter in the urban agglomeration increased sharply and the air quality deteriorated. The trough developed further
257 and a low vortex was formed, which transited across over the study area at 02:00 BST on 5 January 2017 (**Fig. 4d**).
258 The urban agglomeration was then located behind the low vortex and was controlled by a northerly dry, cold air flow
259 (**Fig. 4d**), which illustrated the meteorological conditions in the end of air pollution event. As a result, the air
260 pollutants were rapidly dispersed.

261 The west–east vertical cross-sections of the 24-hour change in temperature and wind vectors (u and w) in the
262 most polluted area (30.75 °N) (**Fig. 5**) and the vertical profiles of temperature and horizontal wind speed (**Fig. 6**)
263 were analyzed to investigate the effects of the low-pressure system on the dynamic and thermodynamic dispersion of
264 air pollutants in the lower troposphere.

265 **Fig.4b** and **4c** shows that the urban agglomeration was located in front of the low-pressure system and was
266 controlled by a southerly warm air flow. There was a descending motion between the top of the boundary layer and
267 500 hPa (**Fig. 5a** and **5b**). Under the effects of warm advection and descending motion, a warming center appeared
268 between 800 and 650 hPa (**Fig. 5a–c**) and the maximum increase in the 24-hour temperature was up to 10 °C (**Fig.**
269 **6a**). Weak cooling occurred below 800 hPa, a strong temperature inversion appeared between 775 and 650 hPa (**Fig.**
270 **6a**), and the stability of the lower troposphere increased. The urban agglomeration was dominated by the
271 low-pressure system for a long time and a long-lasting strong temperature inversion was therefore induced and
272 maintained above the boundary layer. This was different from the temperature inversion that is often seen within the
273 boundary layer in Eastern China (**Ji et al., 2012;Li and Chan, 2016;Li et al., 2012;Wang et al., 2014;Zhang and**
274 **Niu, 2016**). The temperature inversion acted as a lid over the boundary layer, suppressing the dispersion of air
275 pollutants. This lid effect restrained vertical mixing in the atmosphere and the local secondary circulation was
276 therefore confined in the boundary layer, with its center located at about 850 hPa (**Fig. 5a–c**). The horizontal wind

277 speed below 800 hPa was $\leq 2 \text{ m s}^{-1}$ (**Fig. 6b**). These results indicate that vertical mixing and horizontal dispersion
278 were weak, causing accumulation of air pollutants at the ground level. The concentrations of particulate matter then
279 sharply increased to their peak value (**Fig. 3**), generating a heavy air pollution event.

280 A low vortex and trough at 700 hPa transited across the urban agglomeration and a northwesterly dry, cold air
281 flow prevailed (**Fig. 4d**). Under the influence of the cold air flow, a cooling center appeared between 800 and 650
282 hPa (**Fig. 5d**), whereas the air temperature increased below 800 hPa (**Fig. 5d**). As a result, the stability in the lower
283 troposphere was weakened and the strong inversion layer gradually disappeared (**Fig. 6a**). The lid effect above the
284 boundary layer also disappeared, resulting in an increase in the local secondary circulation, the center of which was
285 uplifted to 700 hPa (**Fig. 5d**). The horizontal wind speed below 800 hPa also increased (**Fig. 6b**). The air pollutants
286 were able to disperse over a larger space and the vertical mixing and horizontal dispersion were significantly
287 improved. The air quality improved and the heavy air pollution event ended.

288 To verify whether the mechanism involved in the formation of event 8 is used for the others heavy air pollution
289 events, the vertical profiles of temperature and horizontal wind speed in events 1-7 (**Fig. 7**) were explored during the
290 periods of both the low-pressure system controlling and transited over this urban agglomeration. Similar to the event
291 8, a strong temperature inversion appeared over the study area between 800 and 650 hPa (**Fig. 7a**) when the urban
292 agglomeration was located in the front of low-pressure system and was controlled by a southerly warm air flow at
293 700 hPa. Meanwhile, the horizontal wind speed was low below 800 hPa; the wind speed at all levels below 850 hPa
294 was $\leq 2 \text{ m s}^{-1}$ (**Fig. 7c**). After the low-pressure system had transited across the urban agglomeration, the strong
295 inversion layer above the boundary layer gradually disappeared (**Fig. 7b**), and the horizontal wind speed in the lower
296 troposphere increased (**Fig. 7d**). Therefore, the influencing mechanism of low-pressure system on heavy air pollution
297 events is common in this urban agglomeration.

298 Additionally, ~~composite anomalies~~the anomalies of west-to-east vertical cross-section of 24-hour temperature
299 change and wind vectors (synthesized by u and w) (**Fig. S2**), and the anomalies of temperature vertical profiles (**Fig.**

300 S3) were also analyzed to further investigate the influencing mechanism of low-pressure system on heavy air
301 pollution events. Fig. S2 shows that anomalous warming appeared above the atmospheric boundary layer, while
302 anomalous cooling was observed within the boundary layer when the urban agglomeration was located in front of
303 low-pressure system and was controlled by a southerly warm air flow at 700 hPa. This vertical structure of the
304 anomalies of 24-hour temperature change (Fig. S2) led to an increase in the stability of the lower troposphere. As
305 illustrated in Fig. S3, the positive anomalies of temperature between 1500 m and 3000 m above the ground level
306 increased significantly with height. The maximum value of positive anomalies appeared at about 3000 m and was up
307 to 9 °C. These features revealed that a strong temperature inversion existed above the boundary layer and suppressed
308 the vertical exchange of atmosphere. As a result, the anomalous secondary circulation was also confined in the
309 boundary layer, with its center located at about 925 hPa (Fig. S2). These results of anomalies analysis were
310 consistent with the above analysis for real-time data, and further proved that the influencing mechanism of
311 low-pressure system on heavy air pollution events is credible.

312 From Fig.6 and Fig.7, we also found some interesting features ~~that the effects characterized by the weak effects~~
313 of the transit of low-pressure systems at 700 hPa on the meteorological factors within the boundary layer ~~were weak~~.
314 These features may be related to its deep mountain-basin topography (Fig. 1). Under the effects of the deep
315 mountain-basin topography, wind speed in the boundary layer is often low and ~~with small change magnitudes less~~
316 ~~altered~~ (Chen and Xie, 2012;Huang et al., 2017;Wang et al., 2018), and cold air induced by the transit of
317 low-pressure systems is usually difficult to reach in the ground layer faster (Fig. 5). As a result, the increase
318 ~~magnitudes of~~ wind speed (Fig. 6b, Fig. 7 c and 7d) and ~~the change magnitudes of temperature the degree of change~~
319 ~~in temperature~~ (Fig. 6a, Fig. 7a and 7b) were very small in the boundary layer after the low-pressure system at 700
320 hPa passed. Especially for events 3 and 4, the wind speed decreased and a temperature inversion formed in the
321 boundary layer. These characteristics of the wind and temperature profiles in the boundary layer were the key factors
322 leading to the evolution of boundary layer height as shown in Table 3.

4.2 Impacts of Spring Festival excessive emission on heavy air pollution events

Table 1 shows that events 6 and 7 occurred during the Chinese Spring Festival when the concentration of particulate matter increased sharply. Low concentrations of gaseous pollutants were found throughout these two events, however, which may be related to a reduction in production or the shut-down of factories, as well as lower numbers of vehicles during the week-long Spring Festival (Liao et al., 2017). The centralized letting-off of fireworks during the Chinese Spring Festival played an important part in the sharp increase in the concentrations of particulate matter (Huang et al., 2012; Liao et al., 2017; Shi et al., 2011; Wang et al., 2007). We investigated the impacts of Spring Festival excessive emission on events 6 and 7.

It's noteworthy that the emission of air pollutants increased sharply during this period of deteriorating air quality for events 6 and 7 due to the centralized letting-off of fireworks during the Chinese Spring Festival. What's more, under the effects of low-pressure system, the strong temperature inversion appeared above the atmospheric boundary layer (Fig. 7a) and the horizontal wind speed was low below 800 hPa (Fig. 7c). The combination of excessive emissions with poor dispersion conditions resulted in the maximum daily concentrations of PM₁₀ occurring on the Chinese New Year Day (Table 1). The maximum daily mean PM₁₀ concentration of eight heavy air pollution events occurred in event 7 and was up to 562 $\mu\text{g m}^{-3}$ (Table 1). This shows that the excessive emissions during the short Chinese Spring Festival were able to increase the peak concentrations of particulate matter. Thus, the centralized letting-off of fireworks in the Chinese Spring Festival combined with the impacts of low-pressure system were the main causes of these two events in this region of China.

Unlike in the normal heavy air pollution events, the concentrations of particulate matter began to decrease sharply in event 6 and 7 before the low-pressure system transited over the urban agglomeration (Fig. 8a and 8b), when the strong temperature inversion was still present above the atmospheric boundary layer (Fig. 10), the local secondary circulation was still confined in the atmospheric boundary layer (Fig. 9a and 9b) and the capacity for dispersion has not yet improved significantly (Table 3). To explore the causes of the sharp decrease in PM₁₀

346 concentration for these two events, the effects of fireworks on air quality in Chengdu during Chinese New Year
347 (CNY) from 2013 to 2017 have been investigated. As illustrated in Fig. S4, it is a common phenomenon that PM₁₀
348 concentrations decreased sharply after the letting-off of fireworks stopped during CNY. During 5 days after the
349 letting-off of fireworks stopped, production was reduced, factories were shut-down and the numbers of vehicles were
350 lower due to the week-long holiday of CNY (Liao et al., 2017). As a result, the maximum decrease in the magnitude
351 of PM₁₀ concentration was more than 220 μg m⁻³ and occurred at night from 00:00 BST to 06:00 BST (Fig. S5)
352 which corresponded to the period of the centralized letting-off of fireworks on the Eve of CNY. Based on the above
353 analysis results, we concluded that the sharp decreases in PM₁₀ concentration for events 6 and 7 were mainly
354 attributable to the significant reduction in emissions induced by the letting-off of fireworks stopped and the
355 week-long holiday of CNY. The results showed that time-variations of PM₁₀ concentration during CNY were similar
356 in these five years, even though their meteorological conditions were different. As illustrated in Fig. S4, PM₁₀
357 concentration increased sharply during the periods of the letting-off of fireworks in CNY, and began to decrease
358 significantly after the letting-off of fireworks stopped. These results were consistent with the changes of particulate
359 pollutant concentrations during CNY in other cities of China
360 (http://www.zhb.gov.cn/gkml/hbb/qt/201702/t20170201_395336.htm). It is a common phenomenon that PM₁₀
361 concentrations decreased sharply after the letting-off of fireworks stopped during CNY. Additionally, the diurnal
362 variations of the differences of averaged PM₁₀ concentration in Chengdu between during in the periods of the
363 letting-off of fireworks in CNY (defined as the period from 12:00 BST on the Eve of CNY to 12:00 BST on 1 Lunar
364 January) and 5 days before the letting off fireworks, and between during 5 days after the letting-off of fireworks in
365 CNY and in the periods of the letting-off of fireworks from 2013 to 2017 have been also analyzed (Fig. S5) to
366 evaluate the effects of excessive emission about fireworks on air quality in a better way. The letting-off of fireworks
367 during CNY was observed to have a significant effect on the air quality in Chengdu. Especially during 5 days after
368 the letting-off of fireworks stopped, production was reduced, factories were shut down and the numbers of vehicles

~~were lower due to the week-long holiday of CNY (Liao et al., 2017). As a result, the maximum decrease in the magnitude of PM₁₀ concentration was more than 220 μg m⁻³ and occurred at night from 00:00 BST to 06:00 BST (Fig. S5) which corresponded to the period of the centralized letting-off of fireworks. Based on the above analysis results, we concluded that the sharp decreases in PM₁₀ concentration for events 6 and 7 were mainly attributable to the significant reduction in emissions induced by the letting-off of fireworks stopped and the week-long holiday of CNY. This indicated that these two events were strongly dependent on emissions.~~

5 Conclusions and discussions

We investigated the relationships between low-pressure systems and winter heavy air pollution events in the urban agglomeration of Chengdu, Deyang, and Mianyang in the northwest Sichuan Basin and explored the influence of dry and cold low-pressure systems on winter air quality.

A total of ten heavy winter air pollution events occurred in the urban agglomeration from 1 January 2006 to 31 December 2012 and from 1 January 2014 to 28 February 2017. The meteorological causes of eight of these air pollution events were attributed to dry low-pressure systems (trough and low vortex) at 700 hPa. The schematic diagram in **Fig. 11** shows that a strong temperature inversion appeared above the atmospheric boundary layer because the urban agglomeration was located in front of low-pressure system at 700 hPa and was controlled by a warm southerly air flow. This strong inversion layer acted as a lid over the boundary layer and suppressed the dispersion of air pollutants, confining the local secondary circulation within the atmospheric boundary layer. The horizontal wind speed in the lower troposphere was low. As a result, the space available for the vertical and horizontal dispersion of air pollutants was small. The concentrations of air pollutants increased to their peak values, resulting in heavy air pollution events.

After the low-pressure system had transited across the urban agglomeration, the strong inversion layer above the boundary layer gradually disappeared, resulting in an increase and uplift of the secondary circulation and an increase in the horizontal wind speed in the lower troposphere. The space available for the vertical and horizontal dispersion

392 of air pollutants increased and the concentrations of air pollutants decreased sharply, ending the heavy air pollution
393 event. The centralized letting-off of fireworks during the Chinese Spring Festival was one of the main causes of the
394 heavy air pollution events in this region of China.

395 The urban agglomeration studied here, which is flanked by the eastern slopes of the Tibetan Plateau, is sensitive
396 to low-pressure systems moving east from the plateau (**Feng et al., 2016**). The complex terrain forms local
397 secondary circulations, which have a significant impact on air quality (**Chen et al., 2009; Liu et al., 2009; Miao et al.,**
398 **2015**). We found that the intensity and altitude of the local secondary circulations were markedly affected by the
399 low-pressure system and changes in circulation affected the local air quality. The mechanism of influence of the
400 low-pressure system on the local secondary circulation requires further elaboration using numerical simulation. The
401 centralized letting-off of fireworks during the Chinese Spring Festival significantly affected the air quality (**Huang**
402 **et al., 2012; Liao et al., 2017; Shi et al., 2011; Wang et al., 2007**), especially during some of the heavy air pollution
403 events in the urban agglomeration, although the impact of fireworks on air quality was remarkably different
404 depending on the dispersion conditions (**Li et al., 2006**). Sensitivity research should therefore be carried out using
405 models coupled with detailed meteorological and chemical processes to quantitatively examine the impacts of the
406 centralized emission of air pollutants from the Chinese Spring Festival on local air quality.

407 **Competing interests**

408 The authors declare that they have no conflict of interest.

409 **Acknowledgements**

410 This work was supported by the National Natural Science Foundation of China (91644226, 41575138), the National
411 Key Research Project of China-Strategy on Black Carbon Reduction and Evaluation of the Health Effects of Climate
412 Change (2016YFA0602004), the Improvement on Competitiveness in Hiring New Faculties Fund (2013/14) of The
413 Chinese University of Hong Kong and the Vice-Chancellor's Discretionary Fund of The Chinese University of Hong
414 Kong (4930744). We would like to thank the following departments for the provided data, the Ministry of
415 Environmental Protection of the People's Republic of China, the European Centre for Medium-Range Weather
416 Forecasts, the University of Wyoming and the China Meteorological Administration. Anonymous reviewers who
417 provided comments and suggestions are gratefully acknowledged.

418 **References**

- 419 Bei, N., Li, G., Huang, R. J., Cao, J., Meng, N., Feng, T., Liu, S., Zhang, T., Zhang, Q., and Molina, L. T.: Typical synoptic
420 situations and their impacts on the wintertime air pollution in the Guanzhong basin, China[J], *Atmos. Chem. Phys.*, 16,
421 7373-7387, <https://doi.org/10.5194/acp-16-7373-2016>, 2016.
- 422 Beljaars, A.: Chapter 3: Turbulent transport and interactions with the surface. Part IV: Physical Processes, IFS
423 Documentation, Operational implementation 12 September 2006 Cy31r1 31, ECMWF, Shinfield Park[J], Reading,
424 RG2 9AX, England, 2006.
- 425 Chen, Y., Li, Y., and Zhao, T.: Cause analysis on eastward movement of Southwest China vortex and its induced heavy
426 rainfall in South China[J], *Adv Meteorol.*, 2015, 22, <https://doi.org/10.1155/2015/481735>, 2015.
- 427 Chen, Y., and Xie, S.: Temporal and spatial visibility trends in the Sichuan Basin, China, 1973 to 2010[J], *Atmos. Res.*, 112,
428 25-34, <https://doi.org/10.1016/j.atmosres.2012.04.009>, 2012.
- 429 Chen, Y., Xie, S., Luo, B., and Zhai, C.: Characteristics and origins of carbonaceous aerosol in the Sichuan Basin, China[J],
430 *Atmos. Environ.*, 94, 215-223, <https://doi.org/10.1016/j.atmosenv.2014.05.037>, 2014.
- 431 Chen, Y., Zhao, C., Zhang, Q., Deng, Z., Huang, M., and Ma, X.: Aircraft study of mountain chimney effect of Beijing,
432 China[J], *J. Geophys. Res.*, 114, n/a-n/a, <https://doi.org/10.1029/2008JD010610>, 2009.
- 433 Chen, Z. H., Cheng, S. Y., Li, J. B., Guo, X. R., Wang, W. H., and Chen, D. S.: Relationship between atmospheric pollution
434 processes and synoptic pressure patterns in northern China[J], *Atmos. Environ.*, 42, 6078-6087,
435 <https://doi.org/10.1016/j.atmosenv.2008.03.043>, 2008.

436 Chow, J. C., Watson, J. G., Mauderly, J. L., Costa, D. L., Wyzga, R. E., Vedal, S., Hidy, G. M., Altshuler, S. L., Marrack, D.,
437 Heuss, J. M., Wolff, G. T., Arden Pope Iii, C., and Dockery, D. W.: Health effects of fine particulate air pollution:
438 Lines that connect[J], *J. Air Waste Manage. Assoc.*, 56, 1368-1380, <https://doi.org/10.1080/10473289.2006.10464545>,
439 2006.

440 Deng, T., Wu, D., Deng, X., Tan, H., Li, F., and Liao, B.: A vertical sounding of severe haze process in Guangzhou area[J],
441 *Sci. China Earth Sci.*, 57, 2650-2656, [10.1007/s11430-014-4928-y](https://doi.org/10.1007/s11430-014-4928-y), 2014.

442 Feng, X., Liu, C., Fan, G., Liu, X., and Feng, C.: Climatology and structures of southwest vortices in the NCEP Climate
443 Forecast System Reanalysis[J], *J. Climate.*, 29, 7675-7701, <https://doi.org/10.1175/jcli-d-15-0813.1>, 2016.

444 Fu, S., Sun, J., Zhao, S., and Li, W.: The energy budget of a southwest vortex with heavy rainfall over south China[J], *Adv.*
445 *Atmos. Sci.*, 28, 709-724, <https://doi.org/10.1007/s00376-010-0026-z>, 2011.

446 Gao, Y., Liu, X., Zhao, C., and Zhang, M.: Emission controls versus meteorological conditions in determining aerosol
447 concentrations in Beijing during the 2008 Olympic Games[J], *Atmos. Chem. Phys.*, 11, 12437-12451,
448 <https://doi.org/10.5194/acp-11-12437-2011>, 2011.

449 Gu, Y., and Yim, S. H. L.: The air quality and health impacts of domestic trans-boundary pollution in various regions of
450 China[J], *Environ. Int.*, 97, 117-124, <https://doi.org/10.1016/j.envint.2016.08.004>, 2016.

451 Guo, J., Deng, M., Lee, S. S., Wang, F., Li, Z., Zhai, P., Liu, H., Lv, W., Yao, W., and Li, X.: Delaying precipitation and
452 lightning by air pollution over the Pearl River Delta. Part I: Observational analyses[J], *J. Geophys. Res.-Atmos.*, 121,
453 6472-6488, <https://doi.org/10.1002/2015JD023257>, 2016a.

454 Guo, J., Miao, Y., Zhang, Y., Liu, H., Li, Z., Zhang, W., He, J., Lou, M., Yan, Y., Bian, L., and Zhai, P.: The climatology of
455 planetary boundary layer height in China derived from radiosonde and reanalysis data[J], *Atmos. Chem. Phys.*, 16,
456 13309-13319, <https://doi.org/10.5194/acp-16-13309-2016>, 2016b.

457 Guo, Y., Zeng, H., Zheng, R., Li, S., Barnett, A. G., Zhang, S., Zou, X., Huxley, R., Chen, W., and Williams, G.: The
458 association between lung cancer incidence and ambient air pollution in China: A spatiotemporal analysis[J], *Environ.*
459 *Res.*, 144, 60-65, <https://doi.org/10.1016/j.envres.2015.11.004>, 2016c.

460 He, H., Tie, X., Zhang, Q., Liu, X., Gao, Q., Li, X., and Gao, Y.: Analysis of the causes of heavy aerosol pollution in
461 Beijing, China: A case study with the WRF-Chem model[J], *Particuology*, 20, 32-40,
462 <https://doi.org/10.1016/j.partic.2014.06.004>, 2015.

463 He, J., Gong, S., Yu, Y., Yu, L., Wu, L., Mao, H., Song, C., Zhao, S., Liu, H., Li, X., and Li, R.: Air pollution
464 characteristics and their relation to meteorological conditions during 2014–2015 in major Chinese cities[J], *Environ.*
465 *Pollut.*, 223, 484-496, <https://doi.org/10.1016/j.envpol.2017.01.050>, 2017.

466 Hu, X.-M., Ma, Z., Lin, W., Zhang, H., Hu, J., Wang, Y., Xu, X., Fuentes, J. D., and Xue, M.: Impact of the Loess Plateau
467 on the atmospheric boundary layer structure and air quality in the North China Plain: A case study[J], *Sci. Total*
468 *Environ.*, 499, 228-237, <https://doi.org/10.1016/j.scitotenv.2014.08.053>, 2014.

469 Huang, K., Zhuang, G., Lin, Y., Wang, Q., Fu, J. S., Zhang, R., Li, J., Deng, C., and Fu, Q.: Impact of anthropogenic
470 emission on air quality over a megacity – revealed from an intensive atmospheric campaign during the Chinese

471 Spring Festival[J], *Atmos. Chem. Phys.*, 12, 11631-11645, <https://doi.org/10.5194/acp-12-11631-2012>, 2012.

472 Huang, Q., Cai, X., Song, Y., and Zhu, T.: Air stagnation in China (1985–2014): climatological mean features and trends[J],
473 *Atmos. Chem. Phys.*, 17, 7793-7805, <https://doi.org/10.5194/acp-17-7793-2017>, 2017.

474 Ji, D., Li, L., Wang, Y., Zhang, J., Cheng, M., Sun, Y., Liu, Z., Wang, L., Tang, G., Hu, B., Chao, N., Wen, T., and Miao, H.:
475 The heaviest particulate air-pollution episodes occurred in northern China in January, 2013: Insights gained from
476 observation[J], *Atmos. Environ.*, 92, 546-556, <https://doi.org/10.1016/j.atmosenv.2014.04.048>, 2014.

477 Ji, D., Wang, Y., Wang, L., Chen, L., Hu, B., Tang, G., Xin, J., Song, T., Wen, T., Sun, Y., Pan, Y., and Liu, Z.: Analysis of
478 heavy pollution episodes in selected cities of northern China[J], *Atmos. Environ.*, 50, 338-348,
479 <https://doi.org/10.1016/j.atmosenv.2011.11.053>, 2012.

480 Kuo, Y.-H., Cheng, L., and Anthes, R. A.: Mesoscale analyses of the Sichuan flood catastrophe, 11–15 July 1981[J], *Mon.*
481 *Wea. Rev.*, 114, 1984-2003, [https://doi.org/10.1175/1520-0493\(1986\)114<1984:maotsf>2.0.co;2](https://doi.org/10.1175/1520-0493(1986)114<1984:maotsf>2.0.co;2), 1986.

482 Kuo, Y.-H., Cheng, L., and Bao, J.-W.: Numerical simulation of the 1981 Sichuan flood. Part I: Evolution of a mesoscale
483 southwest vortex[J], *Mon. Wea. Rev.*, 116, 2481-2504,
484 [https://doi.org/10.1175/1520-0493\(1988\)116<2481:nsotsf>2.0.co;2](https://doi.org/10.1175/1520-0493(1988)116<2481:nsotsf>2.0.co;2), 1988.

485 Langrish, J. P., Li, X., Wang, S., Lee, M. M. Y., Barnes, G. D., Miller, M. R., Cassee, F. R., Boon, N. A., Donaldson, K., Li,
486 J., Li, L., Mills, N. L., Newby, D. E., and Jiang, L.: Reducing personal exposure to particulate air pollution improves
487 cardiovascular health in patients with coronary heart disease[J], *Environ Health Perspect.*, 120, 367-372,
488 <https://doi.org/10.1289/ehp.1103898>, 2012.

489 Leng, C., Duan, J., Xu, C., Zhang, H., Wang, Y., Wang, Y., Li, X., Kong, L., Tao, J., Zhang, R., Cheng, T., Zha, S., and Yu,
490 X.: Insights into a historic severe haze event in Shanghai: synoptic situation, boundary layer and pollutants[J], *Atmos.*
491 *Chem. Phys.*, 16, 9221-9234, <https://doi.org/10.5194/acp-16-9221-2016>, 2016.

492 Leśniok, M., Małarzewski, Ł., and Niedźwiedź, T.: Classification of circulation types for Southern Poland with an
493 application to air pollution concentration in Upper Silesia[J], *Phys. Chem. Earth Parts A B C.*, 35, 516-522,
494 <https://doi.org/10.1016/j.pce.2009.11.006>, 2010.

495 Li, L., and Chan, P. W.: LIDAR observation and numerical simulation of vortex/wave shedding at the eastern runway
496 corridor of the Hong Kong international airport[J], *Meteorol. Appl.*, 23, 379-388, <https://doi.org/10.1002/met.1562>,
497 2016.

498 Li, L., Li, J., Xin, L., Li, H., and Wei, Q.: Analysis of atmospheric air pollution of Beijing City in Spring Festival period[J],
499 *China Environ. Sci.*, 26, 537-541 (in Chinese), http://manu36.magtech.com.cn/Jweb_zghjcx/CN/ 2006.

500 Li, Y., Chen, Q., Zhao, H., Wang, L., and Tao, R.: Variations in PM₁₀, PM_{2.5} and PM_{1.0} in an urban area of the Sichuan
501 Basin and their relation to meteorological factors[J], *Atmosphere.*, 6, 150, 2015.

502 Li, Y., Yan, J., and Sui, X.: Tropospheric temperature inversion over central China[J], *Atmos. Res.*, 116, 105-115,
503 <https://doi.org/10.1016/j.atmosres.2012.03.009>, 2012.

504 Liao, T., Wang, S., Ai, J., Gui, K., Duan, B., Zhao, Q., Zhang, X., Jiang, W., and Sun, Y.: Heavy pollution episodes,
505 transport pathways and potential sources of PM_{2.5} during the winter of 2013 in Chengdu (China)[J], *Sci. Total*

506 Environ., 584-585, 1056-1065, <https://doi.org/10.1016/j.scitotenv.2017.01.160>, 2017.

- 507 Lim, S. S., Vos, T., Flaxman, A. D., Danaei, G., Shibuya, K., Adair-Rohani, H., AlMazroa, M. A., Amann, M., Anderson, H.
508 R., Andrews, K. G., Aryee, M., Atkinson, C., Bacchus, L. J., Bahalim, A. N., Balakrishnan, K., Balmes, J.,
509 Barker-Collo, S., Baxter, A., Bell, M. L., Blore, J. D., Blyth, F., Bonner, C., Borges, G., Bourne, R., Boussinesq, M.,
510 Brauer, M., Brooks, P., Bruce, N. G., Brunekreef, B., Bryan-Hancock, C., Bucello, C., Buchbinder, R., Bull, F.,
511 Burnett, R. T., Byers, T. E., Calabria, B., Carapetis, J., Carnahan, E., Chafe, Z., Charlson, F., Chen, H., Chen, J. S.,
512 Cheng, A. T.-A., Child, J. C., Cohen, A., Colson, K. E., Cowie, B. C., Darby, S., Darling, S., Davis, A., Degenhardt,
513 L., Dentener, F., Des Jarlais, D. C., Devries, K., Dherani, M., Ding, E. L., Dorsey, E. R., Driscoll, T., Edmond, K., Ali,
514 S. E., Engell, R. E., Erwin, P. J., Fahimi, S., Falder, G., Farzadfar, F., Ferrari, A., Finucane, M. M., Flaxman, S.,
515 Fowkes, F. G. R., Freedman, G., Freeman, M. K., Gakidou, E., Ghosh, S., Giovannucci, E., Gmel, G., Graham, K.,
516 Grainger, R., Grant, B., Gunnell, D., Gutierrez, H. R., Hall, W., Hoek, H. W., Hogan, A., Hosgood, H. D., Hoy, D., Hu,
517 H., Hubbell, B. J., Hutchings, S. J., Ibeanusi, S. E., Jacklyn, G. L., Jasrasaria, R., Jonas, J. B., Kan, H., Kanis, J. A.,
518 Kassebaum, N., Kawakami, N., Khang, Y.-H., Khatibzadeh, S., Khoo, J.-P., Kok, C., Laden, F., Lalloo, R., Lan, Q.,
519 Lathlean, T., Leasher, J. L., Leigh, J., Li, Y., Lin, J. K., Lipshultz, S. E., London, S., Lozano, R., Lu, Y., Mak, J.,
520 Malekzadeh, R., Mallinger, L., Marcenes, W., March, L., Marks, R., Martin, R., McGale, P., McGrath, J., Mehta, S.,
521 Memish, Z. A., Mensah, G. A., Merriman, T. R., Micha, R., Michaud, C., Mishra, V., Hanafiah, K. M., Mokdad, A. A.,
522 Morawska, L., Mozaffarian, D., Murphy, T., Naghavi, M., Neal, B., Nelson, P. K., Nolla, J. M., Norman, R., Olives,
523 C., Omer, S. B., Orchard, J., Osborne, R., Ostro, B., Page, A., Pandey, K. D., Parry, C. D. H., Passmore, E., Patra, J.,
524 Pearce, N., Pelizzari, P. M., Petzold, M., Phillips, M. R., Pope, D., Pope, C. A., Powles, J., Rao, M., Razavi, H.,
525 Rehfuess, E. A., Rehm, J. T., Ritz, B., Rivara, F. P., Roberts, T., Robinson, C., Rodriguez-Portales, J. A., Romieu, I.,
526 Room, R., Rosenfeld, L. C., Roy, A., Rushton, L., Salomon, J. A., Sampson, U., Sanchez-Riera, L., Sanman, E.,
527 Sapkota, A., Seedat, S., Shi, P., Shield, K., Shivakoti, R., Singh, G. M., Sleet, D. A., Smith, E., Smith, K. R.,
528 Stapelberg, N. J. C., Steenland, K., Stöckl, H., Stovner, L. J., Straif, K., Straney, L., Thurston, G. D., Tran, J. H., Van
529 Dingenen, R., van Donkelaar, A., Veerman, J. L., Vijayakumar, L., Weintraub, R., Weissman, M. M., White, R. A.,
530 Whiteford, H., Wiersma, S. T., Wilkinson, J. D., Williams, H. C., Williams, W., Wilson, N., Woolf, A. D., Yip, P.,
531 Zielinski, J. M., Lopez, A. D., Murray, C. J. L., and Ezzati, M.: A comparative risk assessment of burden of disease
532 and injury attributable to 67 risk factors and risk factor clusters in 21 regions, 1990–2010: a systematic analysis for
533 the Global Burden of Disease Study 2010[J], *Lancet.*, 380, 2224-2260,
534 [https://doi.org/10.1016/S0140-6736\(12\)61766-8](https://doi.org/10.1016/S0140-6736(12)61766-8), 2012.
- 535 Liu, S., Liu, Z., Li, J., Wang, Y., Ma, Y., Sheng, L., Liu, H., Liang, F., Xin, G., and Wang, J.: Numerical simulation for the
536 coupling effect of local atmospheric circulations over the area of Beijing, Tianjin and Hebei Province[J], *Sci. China*
537 *Ser. D Earth Sci.*, 52, 382-392, <https://doi.org/10.1007/s11430-009-0030-2>, 2009.
- 538 Lu, C., Deng, Q.-h., Liu, W.-w., Huang, B.-l., and Shi, L.-z.: Characteristics of ventilation coefficient and its impact on
539 urban air pollution[J], *J. Cent. South Univ.*, 19, 615-622, [10.1007/s11771-012-1047-9](https://doi.org/10.1007/s11771-012-1047-9), 2012.
- 540 Luo, M., Hou, X., Gu, Y., Lau, N.-C., and Yim, S. H.-L.: Trans-boundary air pollution in a city under various atmospheric

541 conditions[J], *Sci. Total Environ.*, 618, 132-141, <https://doi.org/10.1016/j.scitotenv.2017.11.001>, 2018.

542 Luo, Y., Lu, D., Zhou, X., Li, W., and He, Q.: Characteristics of the spatial distribution and yearly variation of aerosol
543 optical depth over China in last 30 years[J], *J. Geophys. Res.*, 106, 14501-14513,
544 <https://doi.org/10.1029/2001JD900030>, 2001.

545 MEP: China National Ambient Air Quality Standards, MEP, Beijing, China, 2012.

546 Miao, Y., Liu, S., Zheng, Y., Wang, S., Chen, B., Zheng, H., and Zhao, J.: Numerical study of the effects of local
547 atmospheric circulations on a pollution event over Beijing–Tianjin–Hebei, China[J], *J. Environ. Sci.*, 30, 9-20,
548 <https://doi.org/10.1016/j.jes.2014.08.025>, 2015.

549 Ni, C., Li, G., and Xiong, X.: Analysis of a vortex precipitation event over Southwest China using AIRS and in situ
550 measurements[J], *Adv. Atmos. Sci.*, 34, 559-570, <https://doi.org/10.1007/s00376-016-5262-4>, 2017.

551 Ning, G., Wang, S., Ma, M., Ni, C., Shang, Z., Wang, J., and Li, J.: Characteristics of air pollution in different zones of
552 Sichuan Basin, China[J], *Sci. Total Environ.*, 612, 975-984, <https://doi.org/10.1016/j.scitotenv.2017.08.205>, 2018.

553 Peng, X., and Cheng, L.: A case numerical study on the evolution of the plateau-east-side low vortex and shear line.
554 Part I: Analysis and diagnosis[J], *J. Lanzhou Univ. Nat. Sci.*, 28, 163-168,
555 <https://doi.org/10.13885/j.issn.0455-2059.1992.02.029>, 1992.

556 Qu, Y., Han, Y., Wu, Y., Gao, P., and Wang, T.: Study of PBLH and its correlation with particulate matter from one-year
557 observation over Nanjing, Southeast China[J], *Remote Sens.*, 9, 668, 2017.

558 Quan, J., Gao, Y., Zhang, Q., Tie, X., Cao, J., Han, S., Meng, J., Chen, P., and Zhao, D.: Evolution of planetary boundary
559 layer under different weather conditions, and its impact on aerosol concentrations[J], *Particuology.*, 11, 34-40,
560 <https://doi.org/10.1016/j.partic.2012.04.005>, 2013.

561 Shi, Y., Zhang, N., Gao, J., Li, X., and Cai, Y.: Effect of fireworks display on perchlorate in air aerosols during the Spring
562 Festival[J], *Atmos. Environ.*, 45, 1323-1327, <https://doi.org/10.1016/j.atmosenv.2010.11.056>, 2011.

563 Slingo, J. M.: The development and verification of a cloud prediction scheme for the ECWMF Model[J], *Q. J. Roy. Meteor.*
564 *Soc.*, 113, 899-927, <https://doi.org/10.1002/qj.49711347710>, 1987.

565 Tang, G., Zhu, X., Hu, B., Xin, J., Wang, L., Münkler, C., Mao, G., and Wang, Y.: Impact of emission controls on air quality
566 in Beijing during APEC 2014: lidar ceilometer observations[J], *Atmos. Chem. Phys.*, 15, 743-750,
567 <https://doi.org/10.5194/acp-15-12667-2015>, 2015.

568 Tao, J., Cheng, T., Zhang, R., Cao, J., Zhu, L., Wang, Q., Luo, L., and Zhang, L.: Chemical composition of PM_{2.5} at an
569 urban site of Chengdu in southwestern China[J], *Adv. Atmos. Sci.*, 30, 1070-1084,
570 <https://doi.org/10.1007/s00376-012-2168-7>, 2013a.

571 Tao, J., Zhang, L., Engling, G., Zhang, R., Yang, Y., Cao, J., Zhu, C., Wang, Q., and Luo, L.: Chemical composition of
572 PM_{2.5} in an urban environment in Chengdu, China: Importance of springtime dust storms and biomass burning[J],
573 *Atmos. Res.*, 122, 270-283, <https://doi.org/10.1016/j.atmosres.2012.11.004>, 2013b.

574 Tao, M., Chen, L., Su, L., and Tao, J.: Satellite observation of regional haze pollution over the North China Plain[J], *J.*
575 *Geophys. Res.-Atmos.*, 117, n/a-n/a, [10.1029/2012JD017915](https://doi.org/10.1029/2012JD017915), 2012.

576 Tao, M., Chen, L., Xiong, X., Zhang, M., Ma, P., Tao, J., and Wang, Z.: Formation process of the widespread extreme haze
577 pollution over northern China in January 2013: Implications for regional air quality and climate[J], *Atmos. Environ.*,
578 98, 417-425, <https://doi.org/10.1016/j.atmosenv.2014.09.026>, 2014.

579 Tian, P., Cao, X., Zhang, L., Sun, N., Sun, L., Logan, T., Shi, J., Wang, Y., Ji, Y., Lin, Y., Huang, Z., Zhou, T., Shi, Y., and
580 Zhang, R.: Aerosol vertical distribution and optical properties over China from long-term satellite and ground-based
581 remote sensing[J], *Atmos. Chem. Phys.*, 17, 2509-2523, <https://doi.org/10.5194/acp-17-2509-2017>, 2017.

582 Wang, Q.-W., and Tan, Z.-M.: Multi-scale topographic control of southwest vortex formation in Tibetan Plateau region in
583 an idealized simulation[J], *J. Geophys. Res.-Atmos.*, 119, 11,543-511,561, <https://doi.org/10.1002/2014JD021898>,
584 2014.

585 Wang, T., Nie, W., Gao, J., Xue, L. K., Gao, X. M., Wang, X. F., Qiu, J., Poon, C. N., Meinardi, S., Blake, D., Wang, S. L.,
586 Ding, A. J., Chai, F. H., Zhang, Q. Z., and Wang, W. X.: Air quality during the 2008 Beijing Olympics: secondary
587 pollutants and regional impact[J], *Atmos. Chem. Phys.*, 10, 7603-7615, <https://doi.org/10.5194/acp-10-7603-2010>,
588 2010.

589 Wang, X., Dickinson, R. E., Su, L., Zhou, C., and Wang, K.: PM_{2.5} pollution in China and how it has been exacerbated by
590 terrain and meteorological conditions[J], *Bull. Am. Meteorol. Soc.*, 99, 105-119,
591 <http://dx.doi.org/10.1175/BAMS-D-16-0301.1>, 2018.

592 Wang, Y., Hao, J., McElroy, M. B., Munger, J. W., Ma, H., Chen, D., and Nielsen, C. P.: Ozone air quality during the 2008
593 Beijing Olympics: Effectiveness of emission restrictions[J], *Atmos. Chem. Phys.*, 9, 5237-5251,
594 <https://doi.org/10.5194/acp-9-5237-2009>, 2009.

595 Wang, Y., Yao, L., Wang, L., Liu, Z., Ji, D., Tang, G., Zhang, J., Sun, Y., Hu, B., and Xin, J.: Mechanism for the formation
596 of the January 2013 heavy haze pollution episode over central and eastern China[J], *Sci. China Earth. Sci.*, 57, 14-25,
597 <https://doi.org/10.1007/s11430-013-4773-4>, 2014.

598 Wang, Y., Zhuang, G., Xu, C., and An, Z.: The air pollution caused by the burning of fireworks during the lantern festival
599 in Beijing[J], *Atmos. Environ.*, 41, 417-431, <https://doi.org/10.1016/j.atmosenv.2006.07.043>, 2007.

600 Wei, P., Cheng, S., Li, J., and Su, F.: Impact of boundary-layer anticyclonic weather system on regional air quality[J],
601 *Atmos. Environ.*, 45, 2453-2463, <https://doi.org/10.1016/j.atmosenv.2011.01.045>, 2011.

602 Whiteman, C. D., Hoch, S. W., Horel, J. D., and Charland, A.: Relationship between particulate air pollution and
603 meteorological variables in Utah's Salt Lake Valley[J], *Atmos. Environ.*, 94, 742-753,
604 <https://doi.org/10.1016/j.atmosenv.2014.06.012>, 2014.

605 Wu, P., Ding, Y., and Liu, Y.: Atmospheric circulation and dynamic mechanism for persistent haze events in the
606 Beijing–Tianjin–Hebei region[J], *Adv. Atmos. Sci.*, 34, 429-440, <https://doi.org/10.1007/s00376-016-6158-z>, 2017.

607 Yang, L., Wu, Y., Davis, J. M., and Hao, J.: Estimating the effects of meteorology on PM_{2.5} reduction during the 2008
608 Summer Olympic Games in Beijing, China[J], *Front Environ Sci Eng.*, 5, 331,
609 <https://doi.org/10.1007/s11783-011-0307-5>, 2011.

610 Ye, X., Song, Y., Cai, X., and Zhang, H.: Study on the synoptic flow patterns and boundary layer process of the severe haze

611 events over the North China Plain in January 2013[J], *Atmos. Environ.*, 124, 129-145,
612 <https://doi.org/10.1016/j.atmosenv.2015.06.011>, 2016.

613 Yu, S., Gao, W., Xiao, D., and Peng, J.: Observational facts regarding the joint activities of the southwest vortex and
614 plateau vortex after its departure from the Tibetan Plateau[J], *Adv. Atmos. Sci.*, 33, 34-46,
615 <https://doi.org/10.1007/s00376-015-5039-1>, 2016.

616 Zeng, S., and Zhang, Y.: The effect of meteorological elements on continuing heavy air pollution: A case study in the
617 Chengdu area during the 2014 Spring Festival[J], *Atmosphere.*, 8, 71, <https://doi.org/10.3390/atmos8040071>, 2017.

618 Zhang, J., Luo, B., Zhang, J., Ouyang, F., Song, H., Liu, P., Cao, P., Schäfer, K., Wang, S., Huang, X., and Lin, Y.: Analysis
619 of the characteristics of single atmospheric particles in Chengdu using single particle mass spectrometry[J], *Atmos.*
620 *Environ.*, 157, 91-100, <https://doi.org/10.1016/j.atmosenv.2017.03.012>, 2017.

621 Zhang, J. P., Zhu, T., Zhang, Q. H., Li, C. C., Shu, H. L., Ying, Y., Dai, Z. P., Wang, X., Liu, X. Y., Liang, A. M., Shen, H.
622 X., and Yi, B. Q.: The impact of circulation patterns on regional transport pathways and air quality over Beijing and
623 its surroundings[J], *Atmos. Chem. Phys.*, 12, 5031-5053, <https://doi.org/10.5194/acp-12-5031-2012>, 2012a.

624 Zhang, S.-T., and Niu, S.-J.: Haze-to-fog transformation during a long lasting, low visibility episode in Nanjing[J], *J. Trop.*
625 *Meteorol.*, 22, 67-77, <https://doi.org/10.16555/j.1006-8775.2016.S1.007>, 2016.

626 Zhang, X. Y., Wang, Y. Q., Niu, T., Zhang, X. C., Gong, S. L., Zhang, Y. M., and Sun, J. Y.: Atmospheric aerosol
627 compositions in China: Spatial/temporal variability, chemical signature, regional haze distribution and comparisons
628 with global aerosols[J], *Atmos. Chem. Phys.*, 12, 779-799, <https://doi.org/10.5194/acp-12-779-2012>, 2012b.

629 Zhang, Z., Zhang, X., Gong, D., Kim, S. J., Mao, R., and Zhao, X.: Possible influence of atmospheric circulations on
630 winter haze pollution in the Beijing–Tianjin–Hebei region, northern China[J], *Atmos. Chem. Phys.*, 16, 561-571,
631 <https://doi.org/10.5194/acp-16-561-2016>, 2016.

632
633

634 **Table 1.** Overview of the eight heavy air pollution events affected by dry low-pressure systems.
 635

Event	Most polluted city	Heavy air pollution event		Most polluted day		End date of heavy air pollution event		Other cities with heavy air pollution
		Start and end dates of air pollution event	PM ₁₀ concentration range in this period ($\mu\text{g m}^{-3}$)	Date	PM ₁₀ concentration ($\mu\text{g m}^{-3}$)	Date	PM ₁₀ concentration ($\mu\text{g m}^{-3}$)	
1	Mianyang	13–14 Jan 2006	284–442	13 Jan 2006	442	15 Jan 2006	166	Chengdu
2	Chengdu	29 Jan 2006	407	29 Jan 2006	407	30 Jan 2006	190	None
3	Chengdu	19–23 Dec 2006	348–385	23 Dec 2006	385	24 Dec 2006	246	None
4	Chengdu	21–24 Dec 2007	260–529	23 Dec 2007	529	25 Dec 2007	174	Mianyang
5	Chengdu	18–20 Jan 2009	264–381	19 Jan 2009	381	21 Jan 2009	220	Mianyang
6	Chengdu	3 Feb 2011	403	3 Feb 2011	403	4 Feb 2011	190	None
7	Chengdu	22–31 Jan 2014	282–562	31 Jan 2014	562	1 Feb 2014	207	Deyang
8	Chengdu	1–6 Jan 2017	294–480	5 Jan 2017	480	7 Jan 2017	118	Deyang

636

637

638 **Table 2.** Relative vorticity at 700 hPa during the periods of deteriorating and improving air quality in each of the
 639 eight heavy air pollution events.
 640

Event	Deteriorating air quality		Improving air quality	
	Time (BST)	Relative vorticity ($1 \times 10^{-5} \text{ s}^{-1}$)	Time (BST)	Relative vorticity ($1 \times 10^{-5} \text{ s}^{-1}$)
1	02:00 on 13 Jan 2006	2.58	20:00 on 13 Jan 2006	-0.94
2	02:00 on 29 Jan 2006	4.15	08:00 on 30 Jan 2006	-3.36
3	20:00 on 22 Dec 2006	4.64	14:00 on 23 Dec 2006	-1.09
4	14:00 on 22 Dec 2007	0.59	14:00 on 23 Dec 2007	-0.82
5	02:00 on 19 Jan 2009	1.75	08:00 on 19 Jan 2009	-2.48
6	02:00 on 3 Feb 2011	2.96	14:00 on 3 Feb 2011	3.16
7	02:00 on 31 Jan 2014	9.12	02:00 on 1 Feb 2014	5.49
8	20:00 on 4 Jan 2017	6.49	08:00 on 5 Jan 2017	-5.74

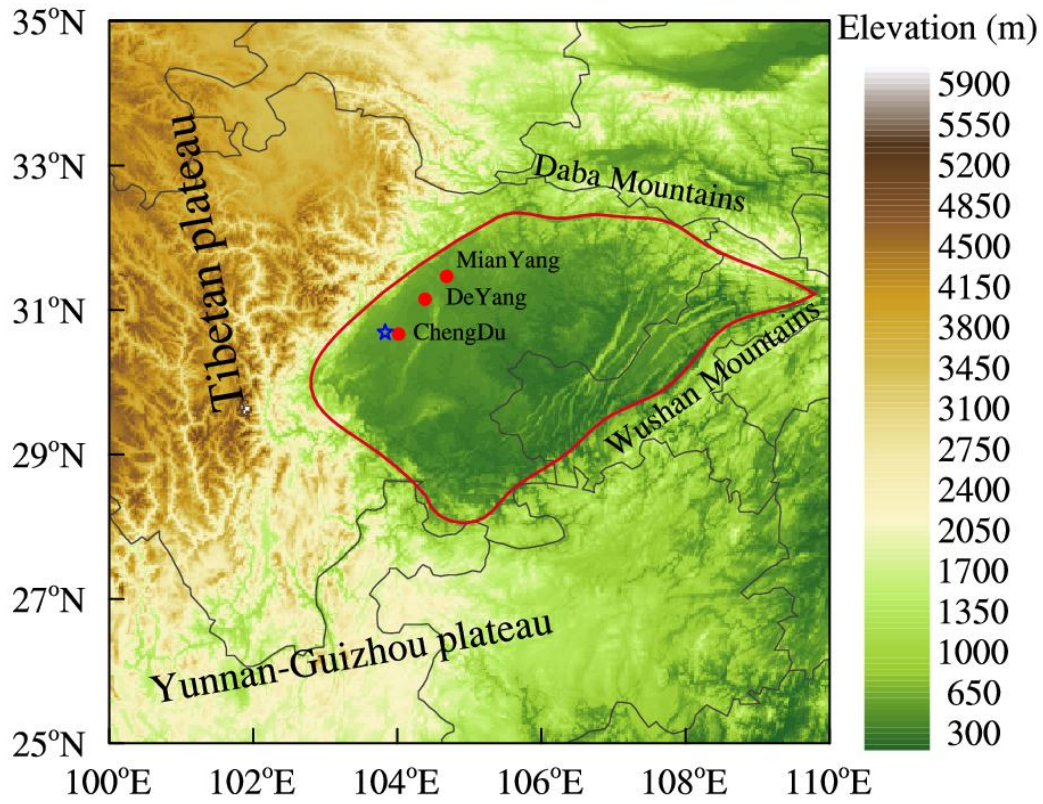
641

642

643 **Table 3.** Height of the atmospheric boundary layer (BLH), lower tropospheric stability (LTS), and mean wind speed
644 (MWS) in the lower troposphere during periods of deteriorating air quality in each of the eight heavy air pollution
645 events, and the differences of them between periods of improving and deteriorating air quality in each event.
646

Event	Deteriorating air quality			Differences between periods of improving and deteriorating air quality		
	BLH (m)	LTS (K)	MWS (m s^{-1})	BLH (m)	LTS (K)	WMS (m s^{-1})
1	278.16	23.13	2.86	144.75	-11.23	0.41
2	375.42	29.45	4.12	139.08	-10.2	1.93
3	279.50	18.54	2.99	-16.45	-5.61	0.34
4	282.61	18.58	1.91	-39.62	-7.23	1.04
5	251.53	19.63	3.11	51.17	-7.88	0.85
6	282.16	25.80	4.22	-16.87	0.55	1.91
7	232.57	25.95	4.21	30.77	-1.97	-1.07
8	266.23	18.88	2.59	107.57	-8.4	0.27

647
648



650

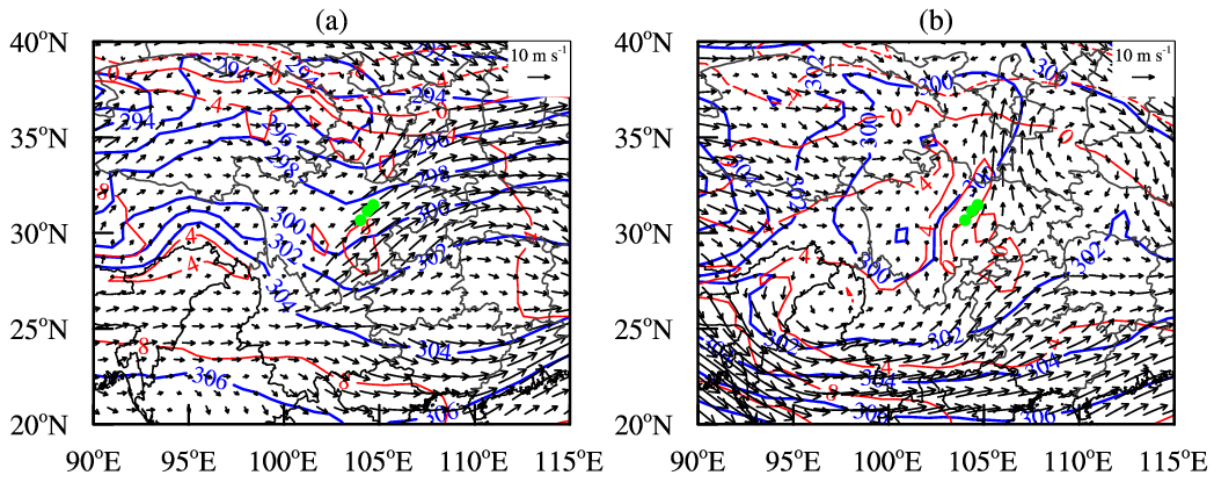
651

Fig. 1 Topographic map (shading, units: m) of the Sichuan Basin (delineated in red) and surrounding areas showing the location of the cities of Chengdu, Deyang, and Mianyang (red dots). The Wenjiang station is marked with blue five-pointed stars. For interpretation of the colors, see web version of this article.

653

654

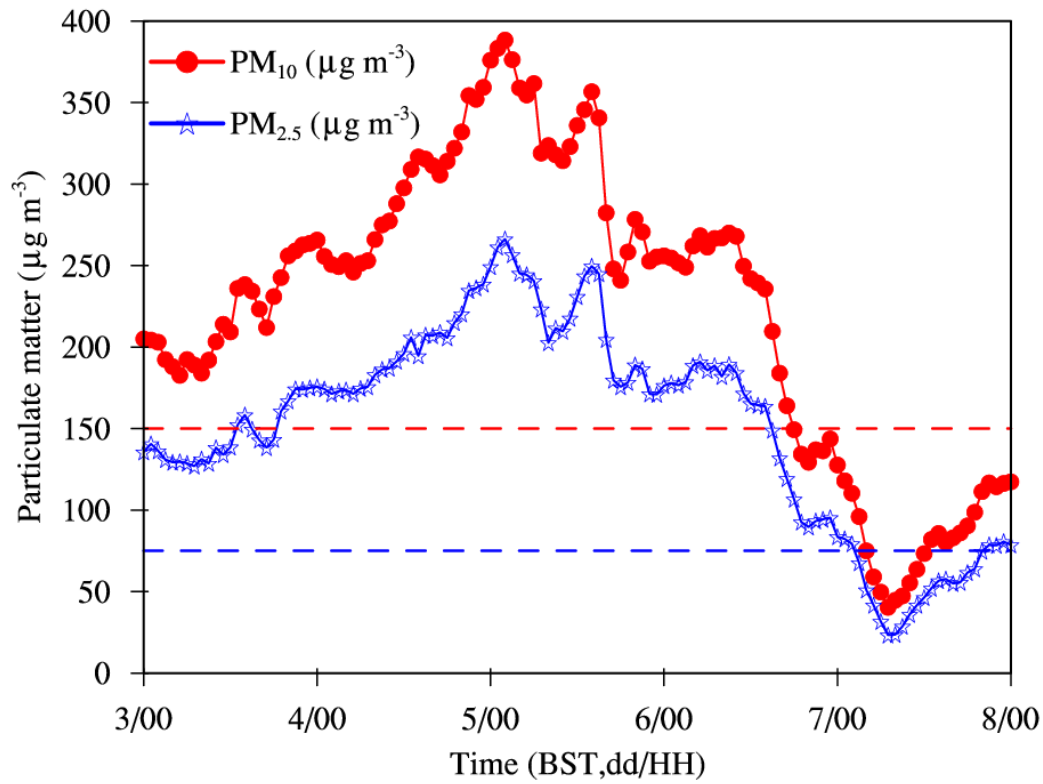
655



656

657 **Fig. 2** Weather maps at 700 hPa based on ERA-Interim daily data showing (a) a trough from event 2 at 20:00 BST
658 on 28 January, 2006 and (b) a low vortex from event 4 at 14:00 BST on 22 December, 2007. The blue lines are
659 isopleths of geopotential height, the red lines are isotherms and the black arrows are wind vectors. The green dots
660 show the location of the urban agglomeration.

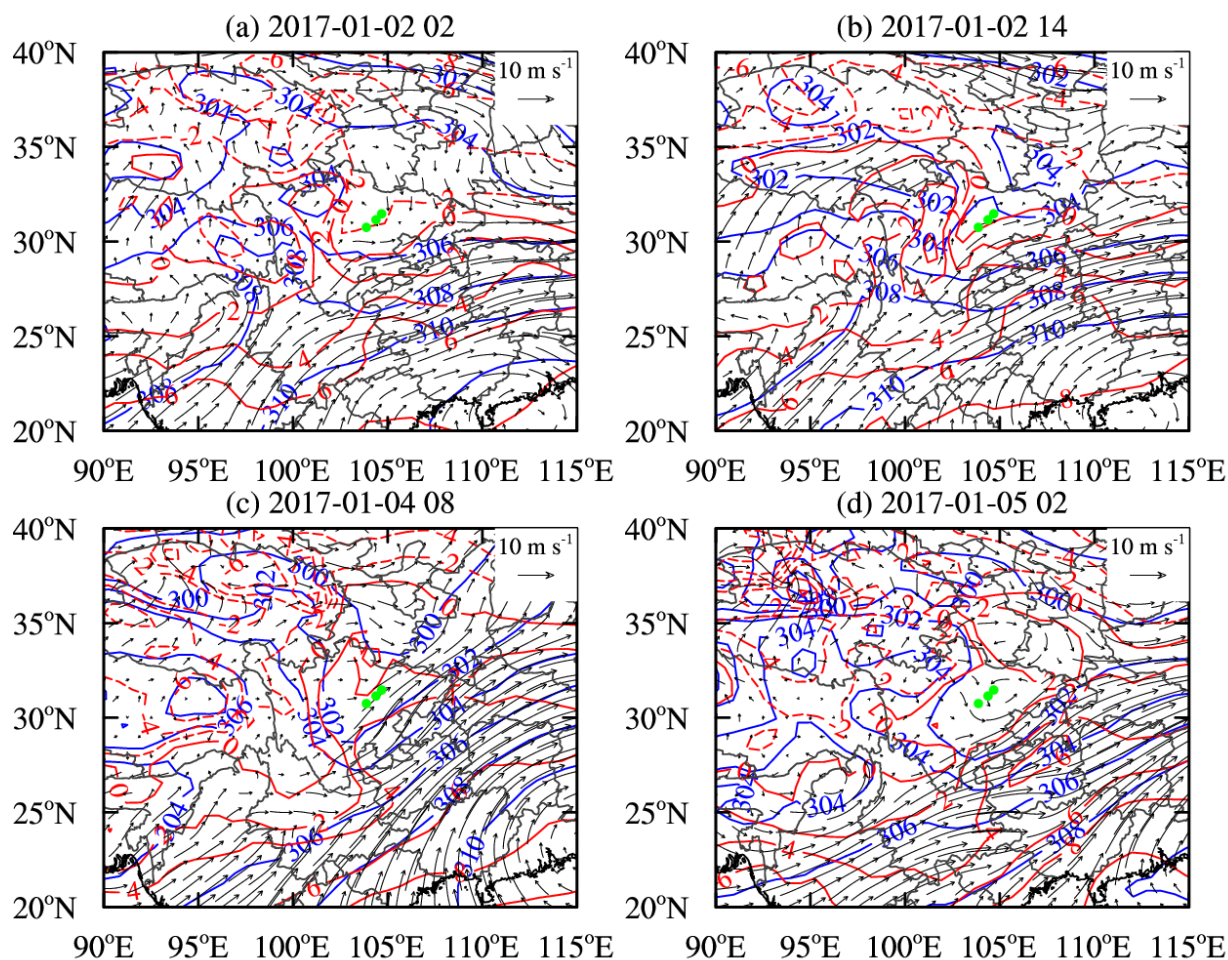
661



663

664 **Fig. 3** Average hourly concentrations of surface PM₁₀ (red solid line) and PM_{2.5} (blue solid line) in the urban
 665 agglomeration from 00:00 BST on 3 January 2017 to 00:00 BST on 8 January 2017 during event 8. The dashed red
 666 line represents Grade II standard of PM₁₀ daily concentration ($150 \mu\text{g m}^{-3}$), the dashed blue line represents Grade II
 667 standard of PM_{2.5} daily concentration ($75 \mu\text{g m}^{-3}$).

668



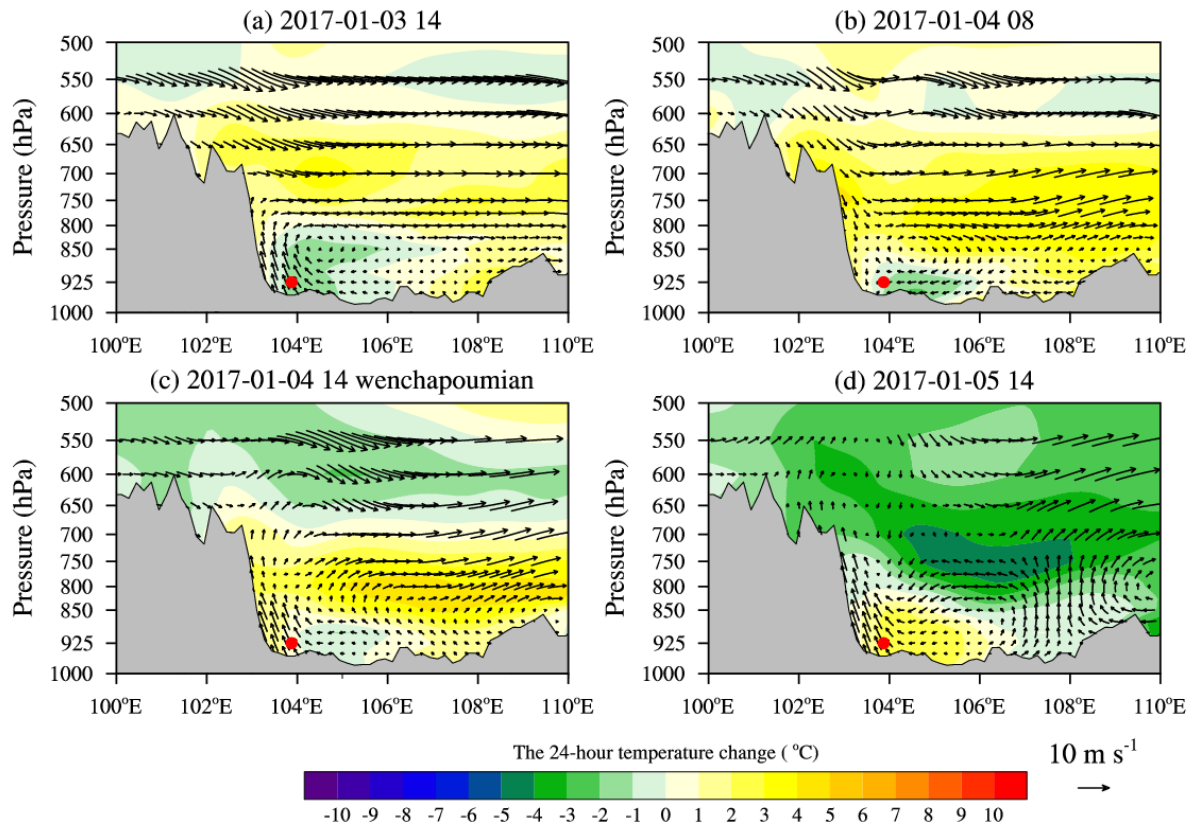
670

671

Fig. 4 Weather maps at 700 hPa for event 8 at (a) 02:00 BST on 2 January 2017, (b) 14:00 BST on 2 January 2017, (c) 08:00 BST on 4 January 2017 and (d) 02:00 BST on 5 January 2017. The blue lines are isopleths of geopotential height, the red lines are isotherms and the black arrows are wind vectors. The green dots show the location of the urban agglomeration.

674

675

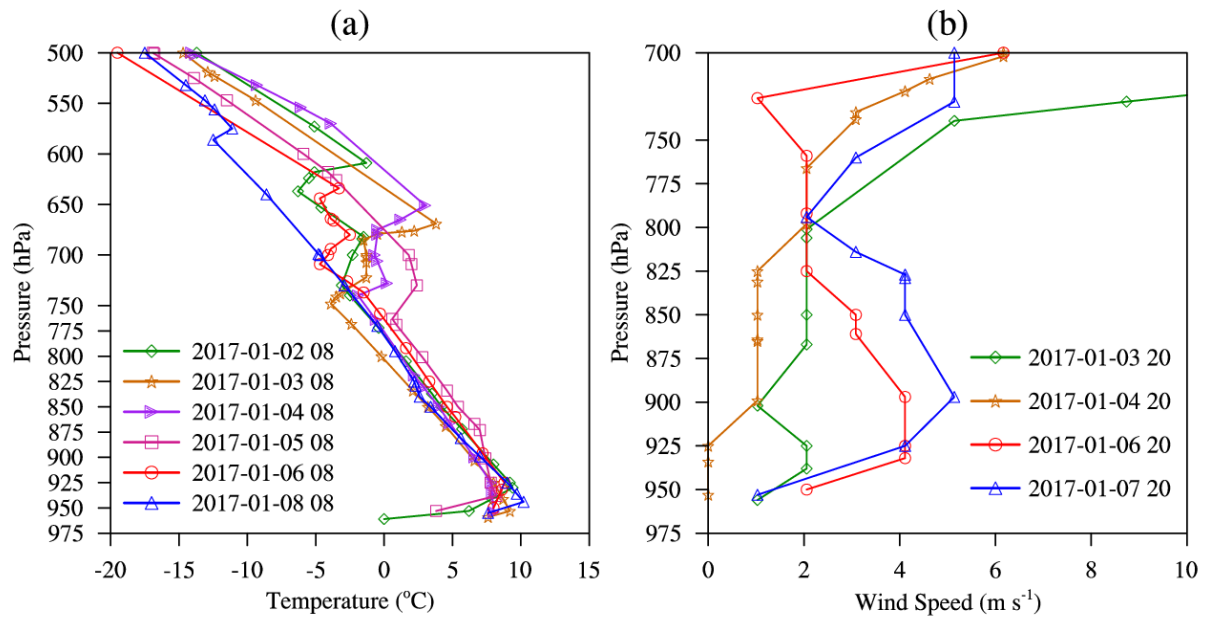


677

678 **Fig. 5** West-to-east vertical cross-sections of 24-hour temperature change (shading, units: °C) and wind vectors
 679 (synthesized by u and w) through the most polluted area (30.75 °N) during event 8 at (a) 14:00 BST on 3 January
 680 2017, (b) 08:00 BST on 4 January 2017, (c) 14:00 BST on 4 January 2017 and (d) 14:00 BST on 5 January 2017
 681 during event 8. Note that the vertical velocity is multiplied by 100 when plotting the wind vectors. The most polluted
 682 area is marked by red solid dots. The gray shading represents the terrain.

683

684



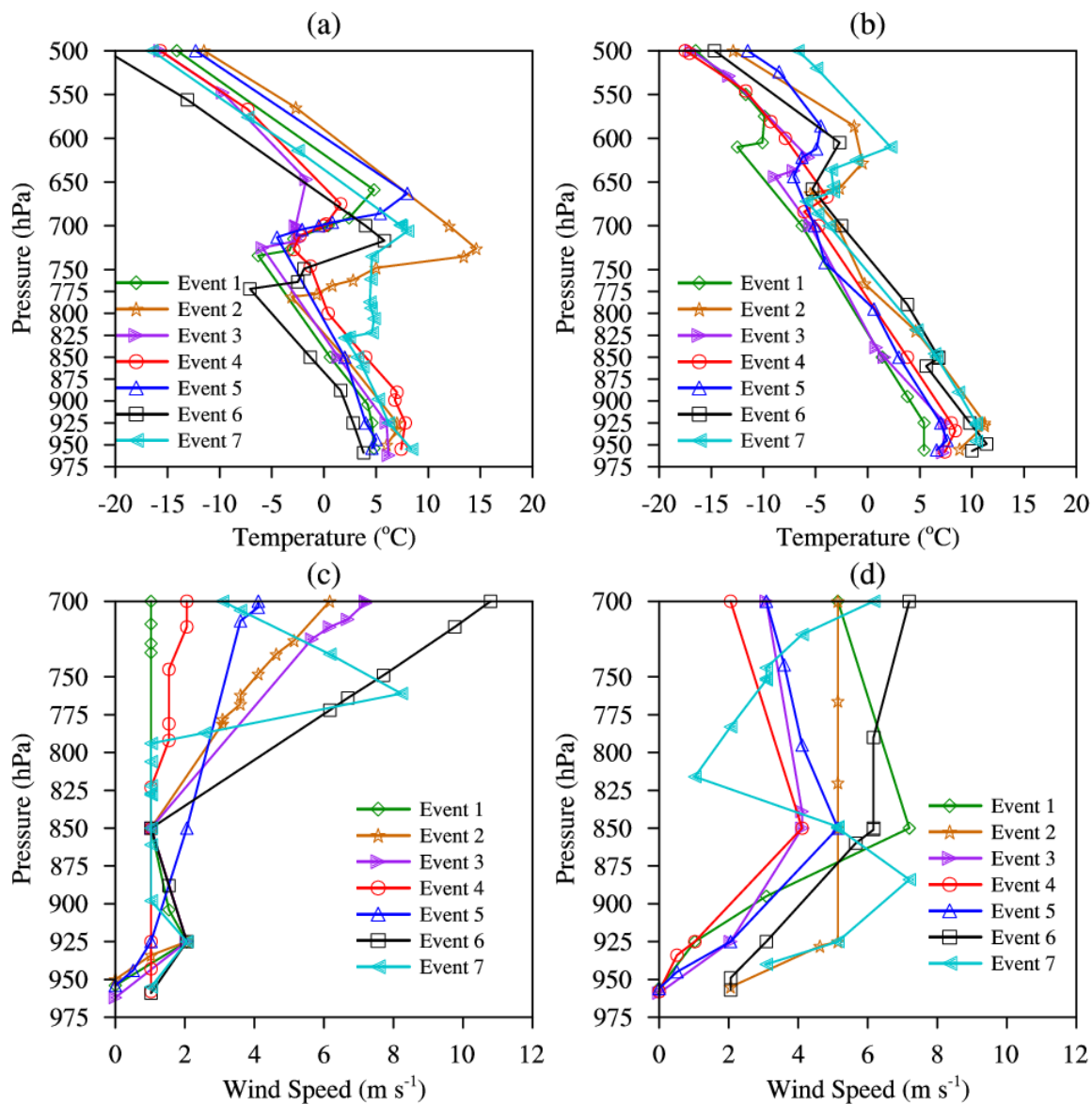
685

686

687

688

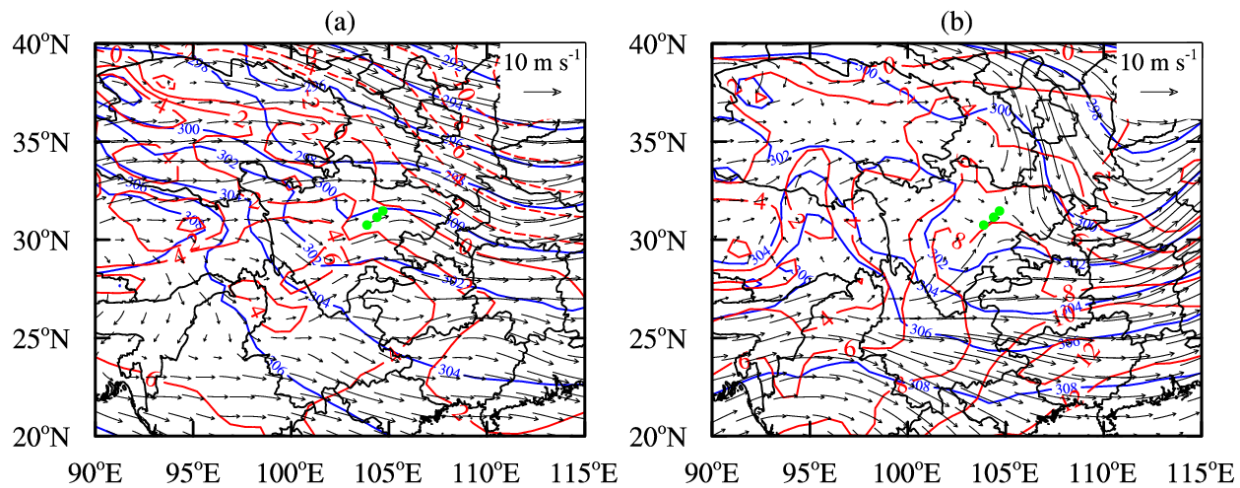
Fig. 6 Vertical profiles of (a) temperature and (b) horizontal wind speed at Wenjiang station (30.75 °N, 103.875 °E, see **Fig. 1**) measured by radiosonde during event 8.



690

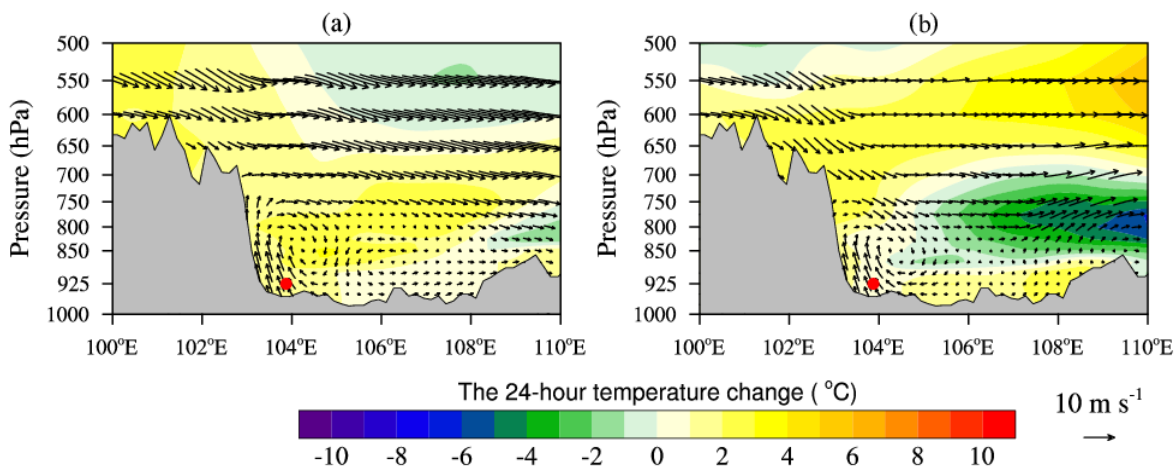
691 **Fig. 7** Vertical profiles of (a) temperature and (c) horizontal wind speed in the urban agglomeration during periods
 692 controlled by the low-pressure system. Vertical profiles of (b) temperature and (d) horizontal wind speed after the
 693 low-pressure system had transited across the urban agglomeration for seven heavy air pollution events (events 1–7).

694



695
696
697
698

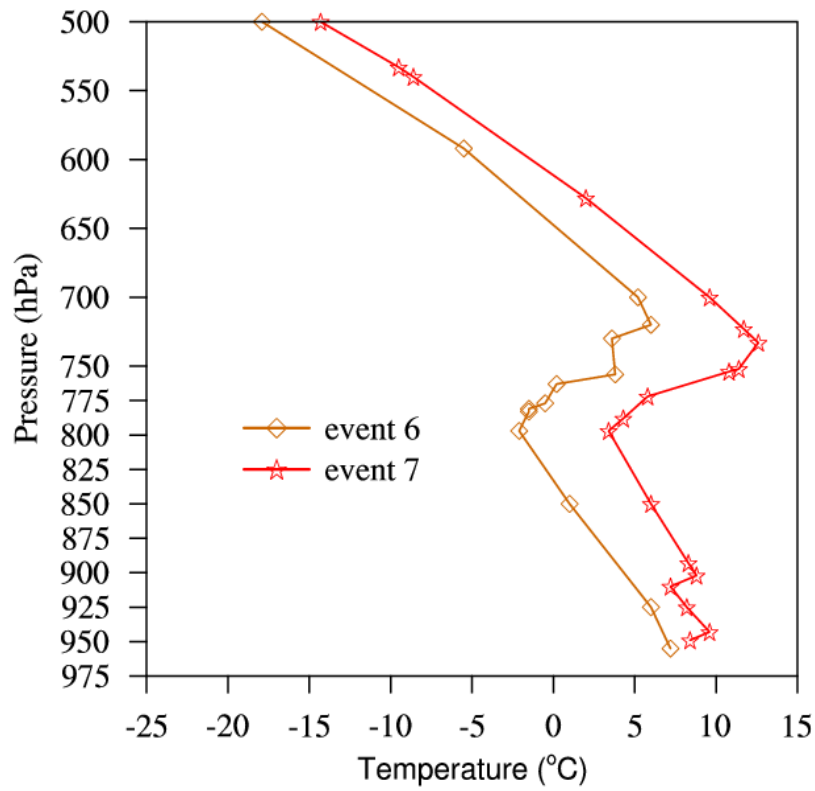
Fig. 8 Weather maps at 700 hPa during periods of improving air quality (a) for event 6 and (b) for event 7. The blue lines are isopleths of geopotential height, the red lines are isotherms and the black arrows are wind vectors. The green dots show the location of the urban agglomeration.



700

701 **Fig. 9** West-to-east vertical cross-sections of 24-hour temperature change (shading, units: $^{\circ}\text{C}$) and wind vectors
 702 (synthesized by u and w) through the most polluted area (30.75°N) during the periods of improving air quality (a)
 703 for event 6 and (b) for event 7. Note that the vertical velocity is multiplied by 100 when plotting the wind vectors.
 704 The most polluted area is marked by red solid dots. The gray shading represents the terrain.

705

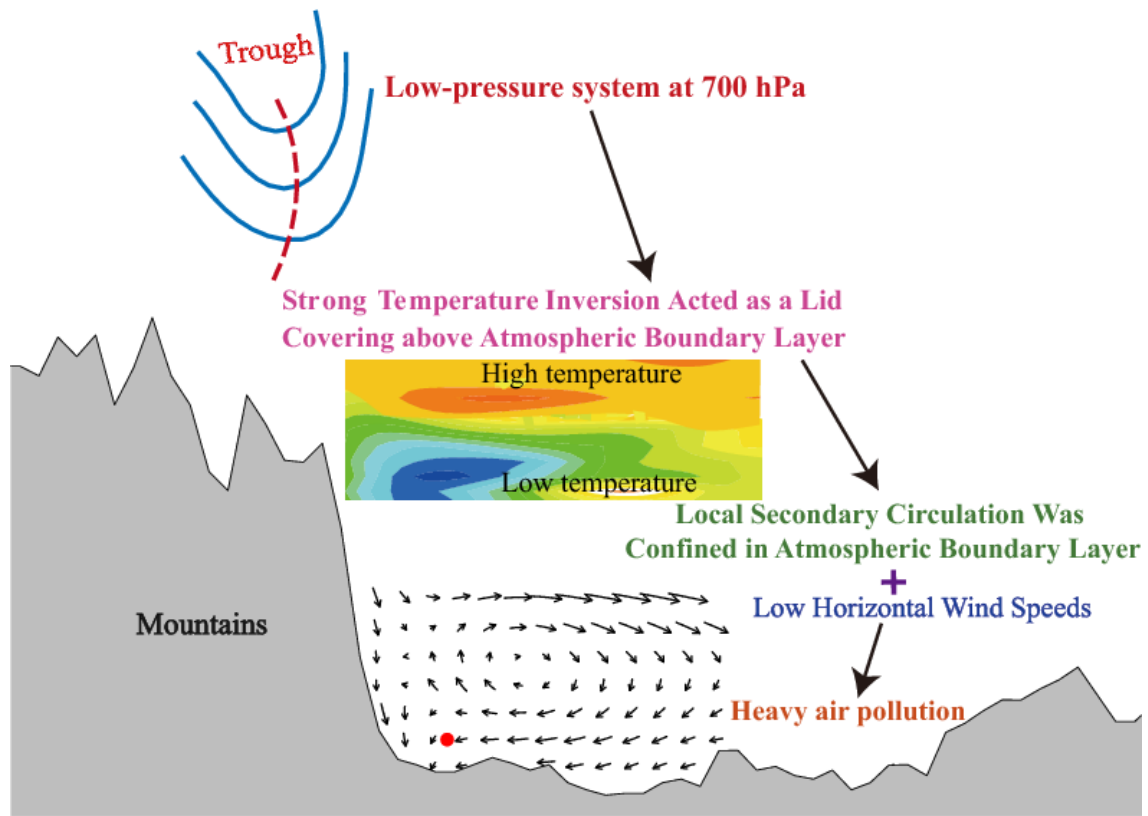


707

708 **Fig. 10** Vertical profiles of temperature at Wenjiang station (30.75 °N, 103.875 °E) measured by radiosonde during
709 periods of improving air quality for event 6 and 7.

710

711



713

714 **Fig. 11** Schematic diagram of the mechanism of influence of a dry low-pressure system on winter heavy air pollution
 715 events in the urban agglomeration.

716

717